

1 **Morphostructural evidence of crustal-scale, active along-strike segmentation of**
2 **the Umbria-Marche Apennines, Italy**

3 **S. Teloni¹, E. Valente^{2*}, A. Ascione², S. Mazzoli¹, P. P. Pierantoni¹, C. Invernizzi¹**

4
5 ¹ School of Science and Technology – Geology Division, University of Camerino, Via Gentile III da Varano, 62032
6 Camerino, MC, Italy

7 ² Department of Earth, Environment and Resources Sciences - DiSTAR, University of Naples Federico II,
8 Complesso Universitario Monte Sant'Angelo, via Vicinale Cupa Cintia 21, 80126, Naples, Italy

9
10 *Corresponding author: Ettore Valente (ettore.valente@unina.it)

11
12 **Abstract**

13 This paper discusses the response of topography and river networks to non-uniform lithology and
14 tectonic forcing in the Umbria-Marche sector of the Apennines fold and thrust belt. We are able
15 to control for variable resistance to erosion of rock types and interpret channel steepness data in
16 terms of rock uplift, discovering a southward increase in the total amount of uplift. Such a trend
17 appears as the large-scale response to uneven vertical motions of different sectors of the
18 mountain ridge and foothills. The general coincidence between sector boundaries and
19 transversal, NE-SW striking faults mapped by seismic interpretation in the outer zone of the fold
20 and thrust belt, suggests that such faults extend to the SW, beneath the allochthonous thrust
21 sheets of the mountainous area. Therefore, it may be inferred that such transversal faults
22 represent long-lived, deeply rooted basement structures compartmentalizing both the axial and
23 the outer zones of the fold and thrust belt. We suggest that differential uplift was essentially
24 controlled by variable amounts of basement thrust displacement characterizing the
25 compartmentalized belt. This interpretation deviates from a more conventional view that uplift of
26 the central Apennines, particularly prominent in the south, is dynamically supported. Our results,
27 besides shedding new light into the active tectonic behavior of a large portion of the Italian

28 peninsula, also provide general insights into the surface response to the differential behavior of
29 crustal blocks produced by along-strike segmentation of active mountain belts.

30

31 **Keywords:** swath profile, chi-plot, normalized steepness index, differential uplift, Apennines

32

33 **1 Introduction**

34 Morphotectonic studies are focused on unraveling the topographic and river network
35 signature of vertical motion distribution (Bishop, 2007; Bull, 2008; Bull and McFadden, 1977;
36 Burbank and Anderson, 2011). The morphotectonic approach has been adopted in different
37 tectonic settings of the world (e.g., Di Biase et al., 2010; Keller and Pinter, 2002; Lanari et al.,
38 2022; Obaid and Allen, 2019; Schildgen et al., 2012; Scotti et al., 2014). The recent development
39 of several GIS and MATLAB based analyses on digital elevation models (Jaiswara et al., 2020;
40 Schwanghart and Kuhn, 2010; Schwanghart and Scherler, 2014; Whipple et al., 2007) has
41 strongly contributed to the large diffusion of morphotectonic analysis at the orogen scale. Several
42 indicators and parameters, such as swath profiles, Ksn index, river long profile and chi plots,
43 have been used to infer the spatial distribution of surface motion in mountain belts (Basilici et
44 al., 2020; Eizenhöfer et al., 2019; Forte et al., 2014; Gallen and Wegmann, 2017; Racano et al.,
45 2021; Pazzaglia and Fisher, 2022). Quantitative analyses of the topography and river network
46 have been applied to the reconstruction of the orogenic growth of the Apennines (e.g., Ascione et
47 al., 2008; Calderoni et al., 2010; D'Agostino et al., 2001; D'Alessandro et al., 2003; Delchiaro et
48 al., 2024; Della Seta et al., 2008; Ferrarini et al., 2021; Lanari et al., 2023; Mayer et al., 2003;
49 Miccadei et al., 2017; Pazzaglia and Fisher, 2022; Piacentini and Miccadei 2014; Racano et al.,
50 2020; Sembroni et al., 2020; Vannoli et al., 2004). Among the main findings of these works is
51 the identification of an uneven uplift along the strike of the mountain range. Multiple datasets
52 and observations point out that the central Apennines are uplifting faster than the northern
53 sectors of the belt, at least since Quaternary times. These datasets include stable isotopes (San
54 Jose et al., (2020), U-Th-He cooling ages (Fellin et al., 2022), geophysical and geodetic datasets
55 (Faccenna et al., 2014; Serpelloni et al., 2013) and linear inversion of river long profiles
56 (Pazzaglia and Fisher, 2022; Racano et al., 2024). The uneven uplift in the Apennines is related
57 to deep processes (e.g., Lanari et al., 2023; Racano et al., 2024). This suggests that the
58 topography of the Apennines is dynamically sustained, thus implying a major role of deep (i.e.,

59 mantle-related) geodynamic processes (D'Agostino et al., 2001; Faccenna et al., 2014; Fellin et
60 al., 2022). In this study, we challenge the idea that large-scale geodynamics is driving non-
61 uniform uplift in the Apennines and suggest that lithospheric, rather than sub-lithospheric mantle
62 processes, are dominant in this active plate boundary setting.

63 With the aim of obtaining further constraints on the pattern of the long-term uplift of the
64 central Apennines, we performed a large-scale morphotectonic analysis of the topography and
65 river network features of the Adriatic slope of the Umbria-Marche Apennines. The Umbria-
66 Marche Apennines and Foothills (UMAF) are characterized by a marked lithological variability
67 and an almost systematic association of carbonate rocks and arenaceous-marly-clayey deposits
68 with the main ridges and topographic lows, respectively. Bearing in mind that the recognition of
69 active tectonic perturbations rests on the identification of the control exerted by lithology on the
70 parameters of topography and drainage network (e.g., Bernard et al., 2019; Clementucci et al.,
71 2022; Pazzaglia et al., 1998; Seagren and Schoenbohm, 2019; Stock and Montgomery, 1999), we
72 compared the results of our morphotectonic analysis with the spatial distribution of outcropping
73 rock types and tectonic structures. The comparison allowed us to define the extent to which the
74 lithological inhomogeneity affects the morphometric parameters of the drainage network. The
75 resulting, unmasked tectonic signal reveals much of the pattern of the large scale along-strike
76 variability of vertical motions. This, in turn, may have implications on seismicity distribution,
77 thus providing new insights into the active tectonic behavior of a large sector of the Italian
78 peninsula.

79 **2 Tectonic framework of the study area**

80 The study area is located in the central–eastern sector of the Italian peninsula (Fig. 1),
81 within the UMAF, which forms part of the peri-Mediterranean Alpine orogenic belt. The
82 Apennines are an arcuate, mostly NW-SE striking fold and thrust belt (Calamita et al., 1994),
83 which evolved during the Neogene in the frame of Africa-Eurasia plate convergence since the
84 Late Cretaceous (Dewey et al., 1989; Mazzoli and Helman, 1994; Turco et al., 2021). Since the
85 Late Miocene, back-arc extension in the hinterland (Tyrrhenian Sea) was coeval with thrusting in
86 the frontal part of the belt (e.g., Butler et al., 2004). Therefore, the Apennines represent a
87 mountain belt characterized by diverse, active geodynamic processes. Defining the relative
88 importance of dynamic (circulating sub-lithospheric, ductile mantle) and tectonic (lithospheric)

89 processes to the building of topography may be difficult (Faccenna et al., 2014). Extension and
90 crustal thinning in the western side of the orogen are well established, as are tectonic accretion
91 and crustal thickening in the eastern side (Butler et al., 2004). However, variable uplift rates and
92 building of topography along the strike of the mountain belt appear to be associated with
93 differential vertical motion of crustal blocks bounded by transversal faults (Calamita et al., 1994;
94 Calamita and Pizzi, 1994). These, in turn, could be variably related with deeper geodynamic
95 processes such as the lateral and vertical propagation of lithospheric tears, slab segmentation and
96 break-off (Ascione et al., 2012; Chiarabba, 1995; Cinque et al., 1993; Lucente et al., 1999; Mele
97 et al., 1998; Montuori et al., 2007; Spakman, 1990; Spakman and Wortel, 2004; Westaway,
98 1993; Wortel and Spakman, 2000; Piromallo and Morelli, 2003).

99 **2.1 Geological and morphostructural setting**

100 The tectonic evolution of the study area consists of three main stages:

101 (1) Pre-orogenic stage (Trias-Paleogene): the Adria rifted continental margin hosted a
102 carbonate platform that was dissected by faulting during the second part of the Early Jurassic,
103 leading to the development of a series of horsts and grabens/half grabens accompanied by
104 transversal oblique-slip transfer faults segmenting the extensional system (Centamore et al.,
105 2002; Centamore and Rossi, 2009; Mazzoli et al., 2005; Pierantoni et al., 2013; Scisciani et al.,
106 2014). Rifting followed by thermal subsidence allowed the deposition of the well-bedded,
107 calcareous-marly Umbria-Marche sedimentary succession (Centamore et al., 2002).

108 (2) Syn-orogenic stage (Miocene-Pliocene): the various sectors of the study area were
109 progressively involved in the fold and thrust belt from west to east, as shown by synorogenic
110 siliciclastic deposits filling a migrating foreland basin system (Centamore et al., 2002). The
111 basement is also involved in the thrust system (e.g., Coward et al., 1999). Transversal faults
112 (probably inherited from the pre-orogenic stage) also controlled differential shortening in
113 adjacent crustal sectors (Calamita et al., 1994; Calamita and Pizzi, 1994).

114 (3) Late-orogenic stage: a general eastward migration of the thrust front toward the foreland
115 characterized the Pliocene to present time (Barchi et al., 2012; Patacca et al., 1990). The
116 hinterland and then the axial zone of the Umbria-Marche Apennines were affected by extension
117 generating NW-SE-striking crustal normal faults (Barchi and Mirabella, 2009; Dewey, 1988;
118 Doglioni, 1995; Keller et al., 1994). Extensional basins host continental deposits (e.g. Gubbio,

119 Norcia and Colfiorito basins; Brogi et al., 2014; Cipollari et al., 1999; Cosentino et al., 2017;
120 Doglioni et al., 1998; Galadini and Messina, 2001; Mancini et al., 2005; Martini and Sagri,
121 1993), while active thrusts in the Adriatic offshore are buried by thick Pliocene-Quaternary
122 foreland basin deposits (e.g., Santini et al., 2021; Fig. 2) whose sedimentation rate largely
123 exceeds thrust slip rates (e.g., Basili and Barba, 2007; Pezzo et al., 2024).

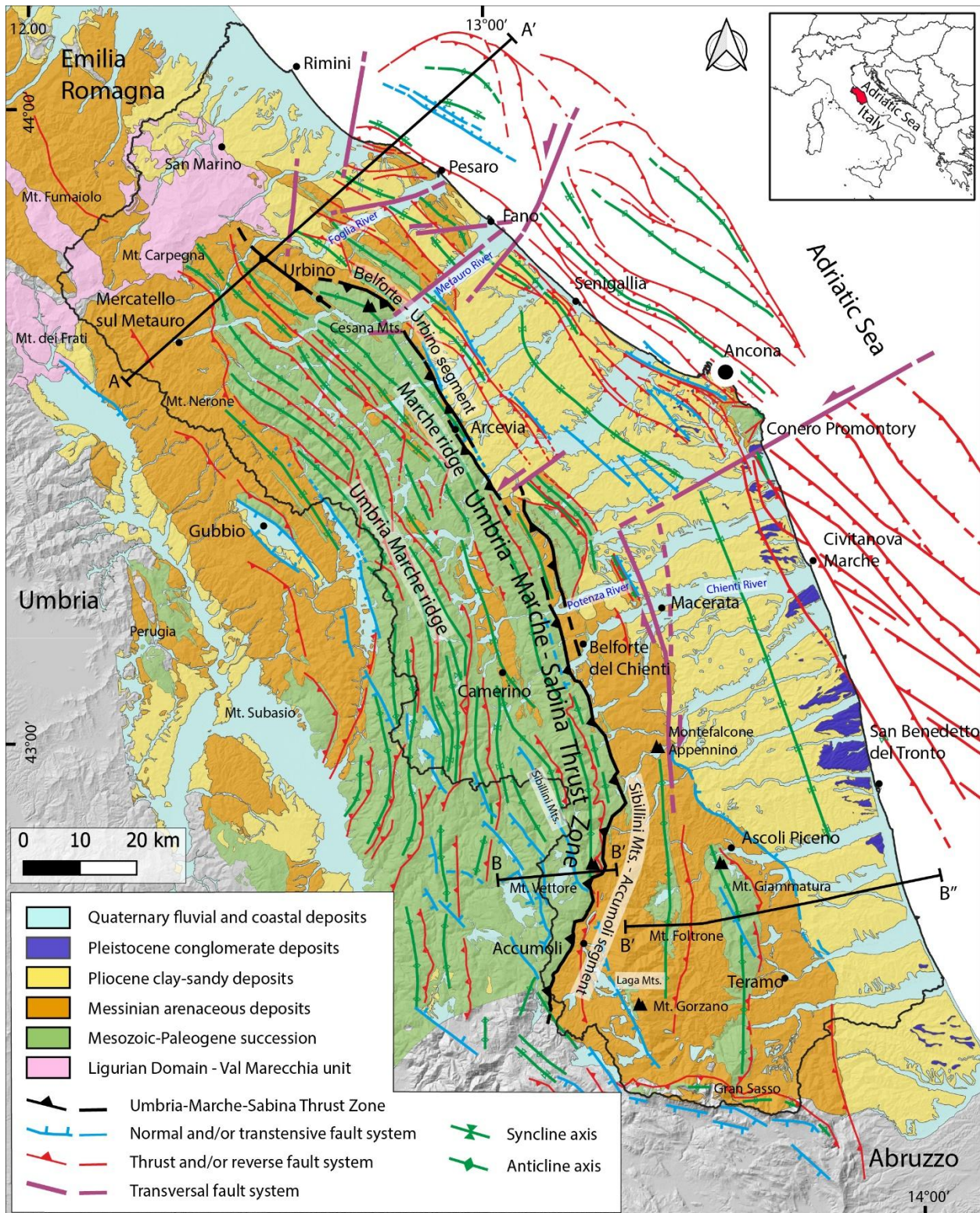
124 The western (i.e., inner) sector of the UMAF includes two anticlinal ridges known as the
125 Umbria-Marche ridge (UMR) and the Marche ridge (MR) (Fig. 1). These ridges expose the
126 Mesozoic-Paleogene Umbria-Marche succession (a calcareous and marly succession with
127 thickness ranging between 1000 and 2000 m) at elevations locally exceeding 2000 m. The
128 intervening valley is a broad synclinorium cored by Upper Miocene terrigenous deposits (Fig. 1).
129 In the eastern (i.e., outer) sector of the UMAF, folds and thrusts exposed at the surface involve
130 mainly the Messinian siliciclastic succession (ranging in thickness from a few hundred meters to
131 the north to 3000 m to the south) and marine to continental Plio-Pleistocene terrigenous deposits
132 of the Marche foothills (Fig. 2).

133 Located along the eastern edge of the MR, the Apennines Mountain front is bounded
134 eastward by the Umbria-Marche-Sabina Thrust Zone (UMSTZ; Fig. 1). The UMSTZ is a major
135 thrust fault consisting of several WNW-ESE to NE-SW striking, right-stepping en-échelon
136 segments. Generally, the UMSTZ is composed of two main thrust portions with an overlap zone
137 10 to 20 km wide between the Potenza River and the Chienti River valleys (Fig. 1). The
138 northern, Belforte-Urbino thrust segment has a general NW-SE trend, changing to WNW-ESE
139 north of the Metauro River valley (Fig. 1). The Belforte-Urbino thrust is imaged in two seismic
140 profiles (including the CROP03 deep seismic reflection profile; Barchi et al., 1998; Calamita,
141 1991). It shows offsets ranging from 2 km to 4.5 km (Mazzoli et al. 2005). The latest thrust
142 activity in this section is attributable to the late Messinian (Deiana et al., 2003). The southern,
143 Sibillini Mts. - Accumoli segment (Fig. 1) experienced the maximum horizontal displacements
144 along the UMSTZ, with values of about 10 km (Mazzoli et al. 2005; Fig. 2). This thrust
145 controlled the mountain front during the Messinian deposition of the Laga Fm. The late stages of

146 activity of this thrust occurred during post-evaporitic late Messinian time, with local slip
147 continuing into the Pliocene (Mazzoli et al. 2005, and references therein).

148

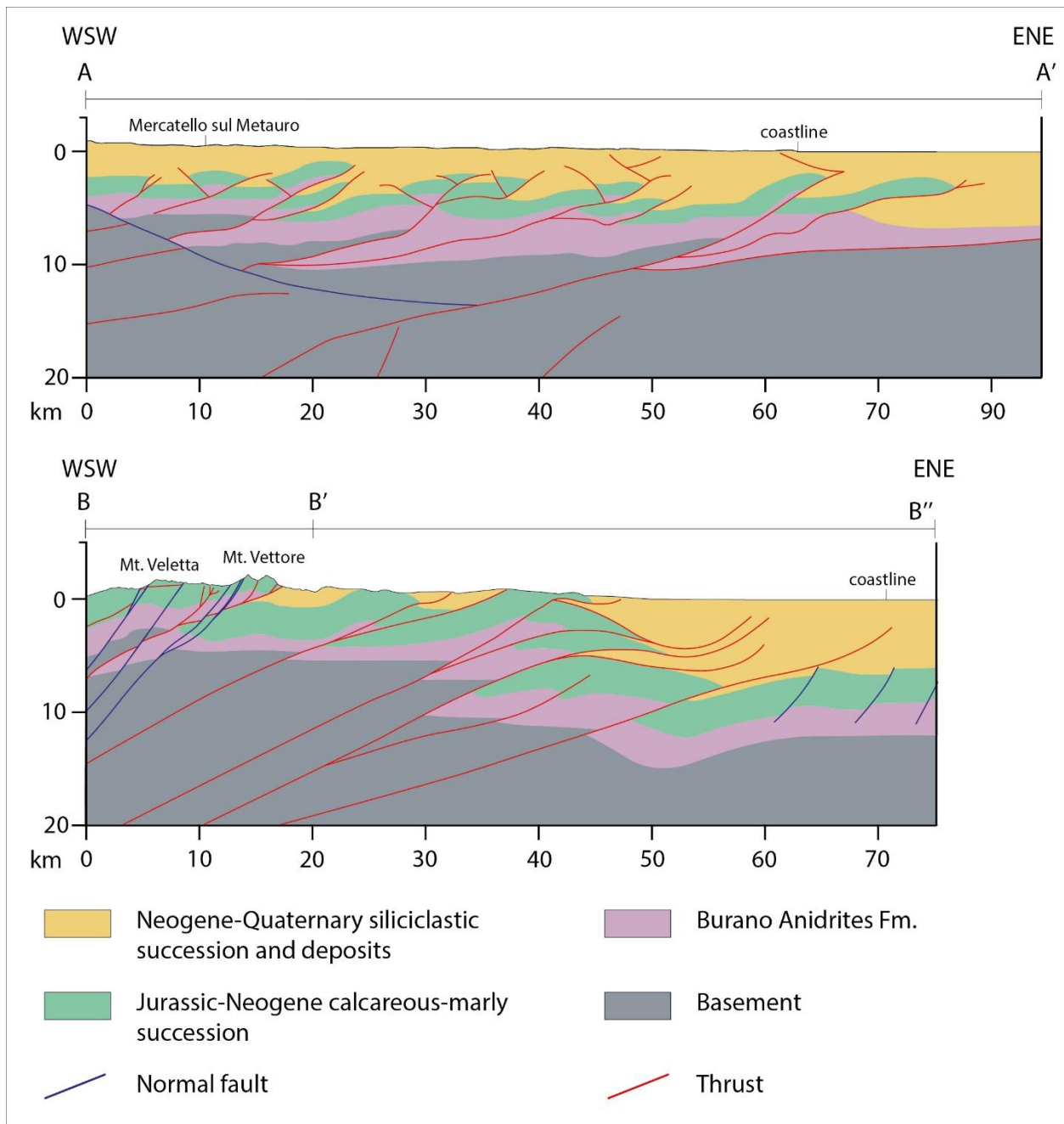
149



150

151 Fig. 1. Structural map of the UMAF and offshore area (modified from Costa et al., 2021 and Pierantoni et al., 2019).

152 Cross-section traces of Fig. 2 are shown (A-A', B-B' and B'-B'' segments).



154

155 Fig. 2. Regional geological sections across the UMAF. Northern section (A-A') modified after Santini et al., 2016.

156 The composite southern section includes segments B-B' (modified after Barchi et al., 1998) and B'-B'' (modified

157 after Pace et al., 2015). Section traces are in Fig. 1.

158 The foothills and coastal areas are traversed by nearly equally-space transverse rivers

159 with headwaters that are subsequent to structure. The river network consists of NE-SW oriented,

160 NE flowing main trunks and related tributaries, flowing within a couple of kilometers to tens
161 kilometers spaced transverse valleys. Most of the NE-SW trending rivers cut the anticline
162 carbonate ridges forming very deeply incised gorges, and locally follow the syncline structures
163 (e.g., the upper Esino River valley) for several kilometers. The long-term evolution of the river
164 network was characterized by superimposition and stream-piracy phenomena in the axial zone of
165 the fold-and-thrust belt, and in the formation of a staircase of strath and fill terraces in the outer
166 zone (i.e., the foothills; Mayer et al, 2003; Nesci et al., 2012; Wegmann and Pazzaglia, 2009).
167 Valley evolution in the foothills followed the mechanism of diverging drainage initially formed
168 on either the top depositional surface of fans or the correlative erosional glacis, whose cone-
169 shaped morphology caused the divergence from the primitive channel (Nesci and Savelli, 2003).
170 Quaternary normal faults are well known to exert a major control on the topography of the study
171 area, particularly in the southern part of the region (e.g., Gentili et al., 2017). Indeed, Della Seta
172 et al. (2008) has highlighted the role of tectonics in shaping the landscape, as several structurally
173 controlled landforms (e.g., rectilinear ridges and valleys, fluvial capture, beheaded valleys,
174 faceted spurs) and offset alluvial terraces suggest a Late Pleistocene activity of NW-SE, WNW-
175 ESE and NE-SW striking fault segments.

176

177 **2.2 Seismicity**

178 The UMAF are the locus of moderate to intense tectonic activity, as shown by (i)
179 instrumental baseline seismicity, (ii) the occurrence of several historical strong earthquakes (e.g.
180 the Mw 6.92, 1703 Valnerina earthquake, which formed part of a 3-earthquakes sequence that
181 struck the whole central Italy; the Mw 6.17, 1741 Fabriano earthquake; the Mw 6.51, 1781 Cagli
182 earthquake and the Mw 6.18, 1799 Camerino earthquake - Castelli and Monachesi, 2001;
183 Monachesi et al., 1991; Rovida et al., 2022; Stucchi et al., 1991), and (iii) recent seismic
184 sequences (e.g. the 1997-1998 Colfiorito seismic sequence with Mw 6.0 main shock - Chiaraluze
185 et al., 2004; the 2016-2017 Amatrice-Visso-Norcia seismic sequence with maximum magnitude
186 6.5 - Civico et al., 2018; EMERGEO working group, 2016). Some of these earthquakes,
187 including the recent Amatrice-Visso-Norcia seismic sequence, are clearly linked to normal faults
188 in the topographic axis of the chain while others, like the Cagli earthquake or Fabriano
189 earthquake that are located further east, are not associated with any clear emergent fault.

190 The seismicity of the Marche foothills and Adriatic offshore is characterized by moderate
191 historical events. The seismotectonic behavior of this sector is consistent with the activity of a
192 highly segmented thrust system (Coward et al., 1999) dominantly including NW-SE striking
193 thrust faults and WSW-ENE striking strike-slip faults (e.g., Basili and Barba, 2007; Costa et al.
194 2021; Mazzoli et al. 2014; Vannoli et al., 2015; Fig. 3).

195
196

197 **3 Material and Methods**

198 A GIS-aided analysis of both topography and river network has been carried out to
199 unravel vertical motion distribution within the UMAF. The 30 m NASA ASTER GDEM V2
200 (<https://asterweb.jpl.nasa.gov/gdem.asp>, last access on 8 December 2022) provided the dataset
201 for morphotectonic analysis through ArcGis 10.8 © and Matlab © software. To compare the
202 results of the morphotectonic analysis with the lithological and active tectonics framework of the
203 UMAF, we constructed a lithological map of the study area and analyzed seismicity distribution
204 using all available instrumental seismic data.

205 **3.1 Topography analysis**

206 Topography is quantified using topographic envelope and sub-envelope maps, which
207 have been coupled with the analysis of seven swath profiles. The spatial distribution of elevation
208 depends on both the resistance to erosion of the outcropping rocks and tectonics (e.g., surface
209 uplift). The maximum elevation mainly reflects the spatial distribution of rock-types, while mean
210 elevation is representative of surface uplift distribution (England and Molnar, 1990) and
211 minimum elevation reflects valley floor distribution (Valente et al., 2019). In addition, spatial
212 variations in uplift may be revealed by local relief distribution, especially in areas where rock
213 types with homogeneous resistance to erosion outcrop (Di Biase et al., 2010). Maximum, mean
214 and minimum elevation maps have been derived by applying a 5x5 km large moving window to
215 the 30 m DTM, whereas relief map has been derived as the difference between maximum and
216 minimum elevation.

217 Swath profiles analysis has been carried out using the SwathProfiler ArcGIS add-in tool (Pérez-
218 Peña et al., 2017). Seven swath profiles, 20 km in width and with different orientations were
219 constructed: five profiles, with SW-NE orientations, are roughly perpendicular to the trend of the
220 UMAF; one profile follows the bending of the UMAF arc, thus including both chain and

221 foreland units; one profile, NW-SE trending, moves within the foothills underlain by foredeep
222 units.

223

224 **3.2 Analysis of the river network**

225 River network analysis included the construction of river longitudinal profiles and
226 transformed river long profiles (chi-plot), which have been coupled with the slope/area analysis
227 to derive the spatial distribution of the normalized channel steepness index (K_{sn}). Analyzed
228 rivers are 18 main trunks that drain from the SW to the NE across the UMAF.

229 We analyzed the river network by means of the Topotoolbox scripts of Matlab (Schwanghart
230 and Kuhn, 2010; Schwanghart and Scherler, 2014) and the Run-Chi profiler script (Gallen and
231 Wegmann, 2017). Slope/area analysis relates channel slope with the drainage area following the
232 equation:

$$233 S = k_s A^{-\theta} \quad (1)$$

234 where S is the channel slope, k_s is the steepness index, A is the drainage area and θ is the
235 concavity index. The analysis is synthesized in a log-log slope vs area diagram with θ being the
236 angle of the regression line and the k_s being the y-intercept. Because small variation in θ may
237 provide significant variation in the y-intercept, to compare basins with different drainage areas a
238 reference concavity must be defined. We determined a reference concavity (θ_{ref}) of 0.59 that
239 derives from averaging concavity values between each of the 18 analyzed drainage basins.
240 Furthermore, a smoothing window of 500 m and a reference drainage area $A_0 = 1 \text{ km}^2$ have been
241 adopted. The resulting steepness index is named K_{sn} (normalized steepness index).

242 The dependence of the K_{sn} index from bedrock lithology is well established in various
243 climatic environments (e.g., Bernard et al., 2019; Das et al., 2022; Fadul et al., 2022). We
244 evaluated such dependency by means of a statistical analysis of the K_{sn} values as a function of
245 lithology and presented the results as a box and whisker plot. The lithological control on
246 parameters of topography and river network may be quantified by defining erodibility value (K)
247 of equation 2. Assuming a simple stream power model where n=1, the K_{sn} values could be
248 converted to erodibility values (K) using $K = E / K_{\text{sn}}$. This analysis would require compiling all
249 available erosion rate data for the study area (Pazzaglia and Fisher, 2022).

250 Bedrock variability at the drainage basin scale may also control the formation of convex
251 upward reaches in the long profiles named knickpoint. These have been classified according to

252 their proximity to contacts between different rock types following the method proposed by
 253 Buscher et al. (2017): knickpoints that are less than 200 m far from lithological contacts have
 254 been classified as “lithology-controlled knickpoints”, whereas knickpoints that are more than 200
 255 m far from lithological contact have been classified as “non-lithology-controlled knickpoints”.

256 Further information about the rivers’ response to external perturbations (i.e., tectonics) may
 257 be revealed by transformed river long profiles (Perron and Royden, 2013; Royden and Perron,
 258 2013). Transformed river long profiles dissecting a uniform rock-type and equilibrated with
 259 uplift have a linear shape, with k_s being the slope of the transformed profiles. To obtain
 260 transformed river long profiles (chi plots), Equation 1 can be rewritten as follows:

$$261 \quad S = \left(\frac{U}{K}\right)^{\frac{1}{n}} A^{-\frac{m}{n}} \quad (2)$$

262 where U is the rock uplift rate, K is an erodibility coefficient, A is the drainage area, and m and n
 263 are constants. Under constant U and K , separating variables in Equation 2 and integrating them,
 264 produces

$$265 \quad z(x) = z(x_b) + \left(\frac{U}{KA_0^m}\right)^{\frac{1}{n}} \chi \quad (3)$$

266 with

$$267 \quad \chi = \int_{x_b}^x \left(\frac{A_0}{A(x)}\right)^{-\frac{m}{n}} dx \quad (4)$$

268
 269 where $z(x)$ is the elevation of an observation point along the river long profile, $z(x_b)$ is the
 270 elevation of the local base level, $A(x)$ is the drainage area at the observation point $z(x)$, A_0 is a
 271 reference drainage area, and m/n is the reference concavity. We set the reference drainage area
 272 (A_0) to 1 km² whereas the smoothing window is 500 m.

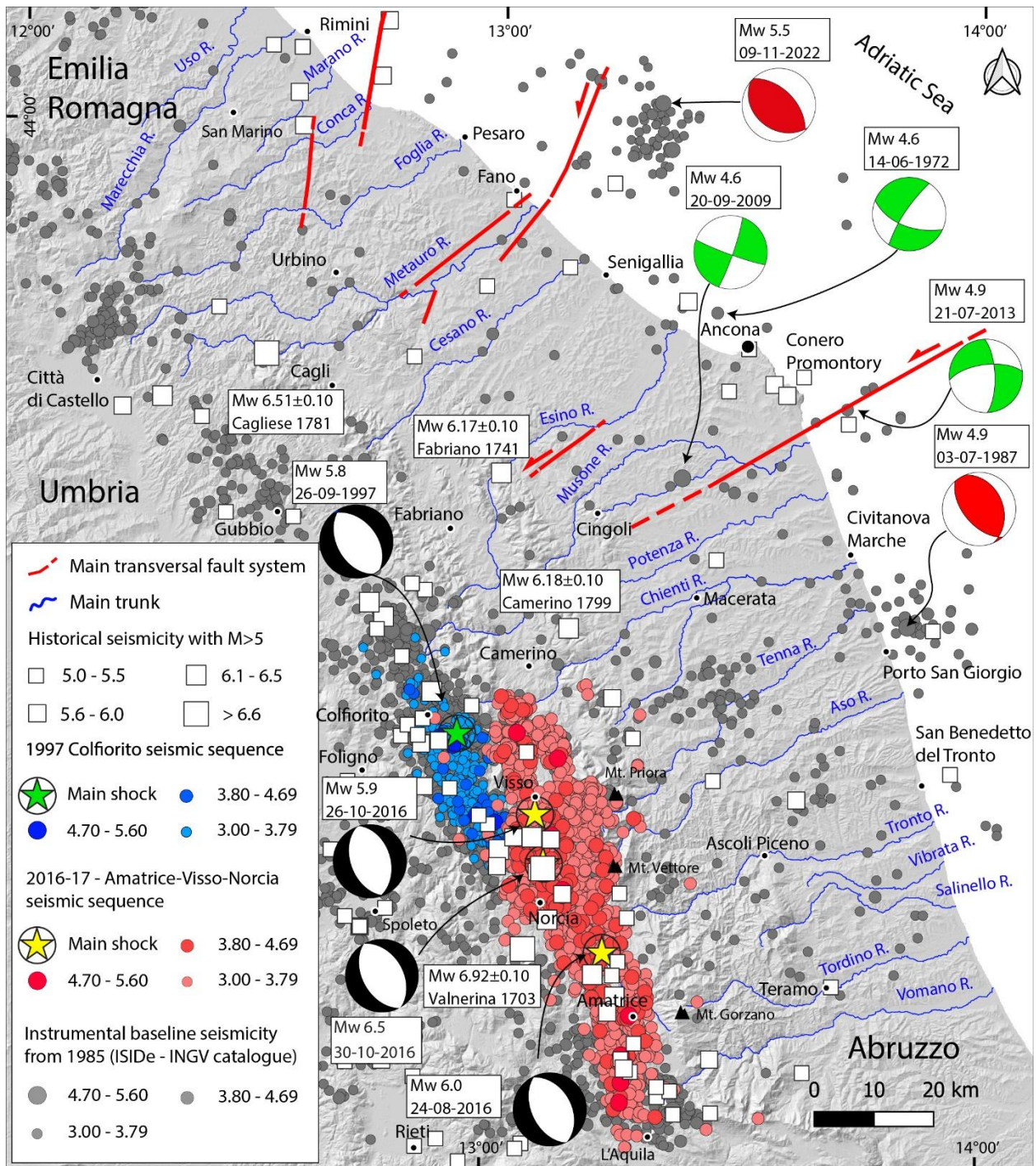
273 In the chi-plot analysis it is crucial the recognition of the best-fit m/n ratio (θ , reference
 274 concavity) at the drainage basin scale, whereas to compare rivers with different drainage areas a
 275 reference concavity must be defined, which derives from averaging the m/n values of all the
 276 analyzed rivers (Perron and Royden, 2013). The best fit m/n ratio at the basin scale has been
 277 derived by the Bayesian optimization script of Topotoolbox (Schwanghart and Kuhn, 2010;
 278 Schwanghart and Scherler, 2014). To compare chi-plots among the 18 investigated rivers we
 279 derived an average reference concavity value of 0.59.

280
281
282
283
284
285
286
287
288
289
290
291
292
293
294
295

4 Results

4.1 Distribution of seismicity in the UMAF

The instrumental seismic data recorded since 1985 from the Italian Seismological Instrumental and Parametric Data-Base (<http://terremoti.ingv.it/iside> ISIDe -INGV, last access on 24 January 2023) and the re-localized earthquakes by INGV Ancona (Cattaneo et al., 2017) have been downloaded and merged together in a new database to analyze seismicity distribution. In this regard, a dataset of 4016 earthquakes data have been selected among more than 70.000 events upon the horizontal error ($erh < 2.5$ km), vertical error ($erz < 2.5$ km) and number of phases of the seismogram (> 8), which are considered reliable to avoid uncertainties due to epicenters position. In this dataset the 2016-2017 Amatrice-Visso-Norcia seismic sequence and the 1997 Colfiorito seismic sequence are also present and differentiated from the baseline seismicity (Fig. 3) through the ZMAP decluster algorithm (Wiemer, 2001).



296
 297 Fig. 3 – Historical (white boxes) and instrumental seismicity with magnitude higher than 3 (circles) for the eastern
 298 central Italy and surrounding area. Red circles show the 2016-2017 Amatrice-Visso-Norcia seismic sequence whereas
 299 yellow stars highlight the main shocks. Blue circles and green stars represent the 1997 Colfiorito seismic sequence
 300 and main shock (Mw 5.8) respectively. Gray circles show other seismic events included in the ISIDe database. Focal
 301 mechanism solutions (black: dominant normal faulting; green: dominant strike-slip faulting; red: dominant reverse

302 faulting) are from ISIDe database (ISIDe Working Group, 2007) and from Mazzoli et al. (2014) and Santini et al.
303 (2011). White squares represent historical seismic events with $M > 5$ (Rovida et al., 2022).

304
305 The map of Fig. 3 shows that earthquakes are mainly clustered in the SW sector of the
306 UMAF (i.e., the Sibillini Mts.), which was struck by the 2016-2017 Amatrice-Visso-Norcia
307 seismic sequence. Both the location of the major historical earthquakes and the spatial
308 distribution of instrumental seismicity confirm the intense tectonic activity along the UMR and
309 the MR. Here, the highest magnitude concentrated in the southern sector, as highlighted by the
310 2016-2017 seismic sequence. Seismic events with magnitude ranging between 3 and 6.5 are
311 generally located along the chain axis and associated with NW-SE striking normal faults,
312 including the Monte Vettore and Monte Gorzano faults. The 2016-2017 aftershocks are confined
313 between the Chienti River valley to the north and the Vomano River valley to the south.
314 Earthquake focal mechanism solutions available from the ISIDe database (ISIDe Working
315 Group, 2007) indicate a predominant normal faulting along the Apennines (Fig. 3), with NE-SW
316 oriented T-axis in agreement with the Quaternary tectonics of this sector (Frepoli and Amato,
317 1997).

318 The Marche foothills and Adriatic offshore are characterized by moderate historical
319 events and low to moderate instrumental seismicity (e.g., Mw 5.83, 1930 Senigallia earthquake,
320 Mw 4.68, 1972 Ancona earthquake, Mw 4.90, 1987 Porto San Giorgio earthquake, Mw 4.00,
321 2022 Costa Marchigiana-Picena earthquake; ISIDe Working Group, 2007; Monachesi et al.,
322 1991; Rovida et al., 2022). Earthquake focal mechanism solutions include NW-SE striking thrust
323 faulting and WSW-ENE oriented strike-slip faulting (e.g., Basili and Barba, 2007; Costa et al.
324 2021; Costa et al. 2023; Mazzoli et al. 2014; Vannoli et al., 2004, 2015; Fig. 3).

325

326 **4.2 Lithological map of the UMAF**

327 Detecting the lithological signature on topography and drainage network metrics is
328 crucial to avoid errors in interpreting the spatial distribution of these parameters as due only to
329 tectonics. For this reason, we modified the 1:250.000 geologic map of the northern Apennines
330 (Conti et al., 2020), and lithostratigraphic units have been grouped in eleven categories according
331 to their lithology and stratigraphical position. The derived simplified geological map (Fig. 4) has

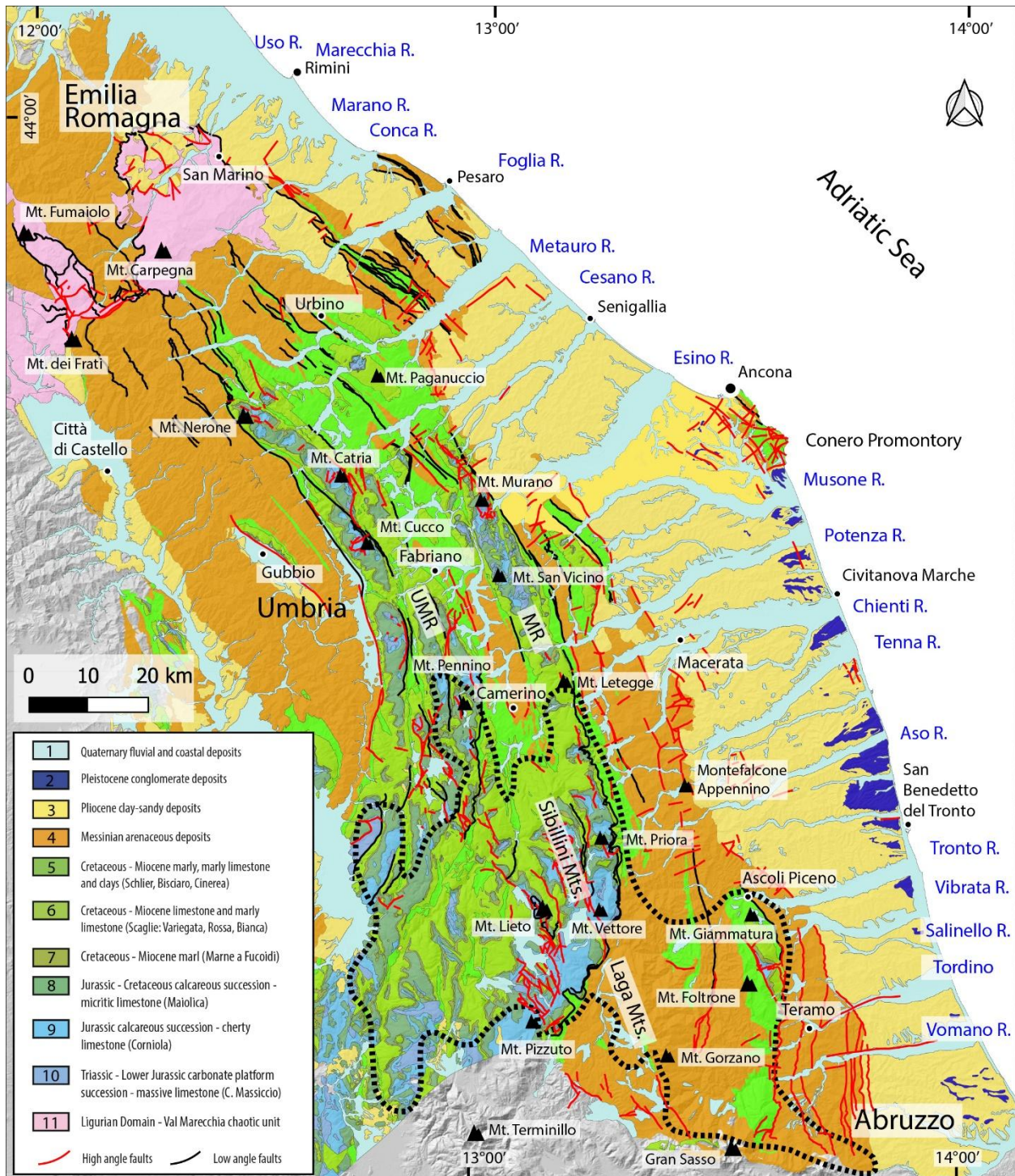
332 been used as a reference frame for interpreting the results of topography and river network
333 analyses.

334 In the northernmost sector of the UMAF, highly allochthonous tectonic units belong to the
335 Ligurian domain. These units are represented by the Val Marecchia ‘chaotic’ units (unit 11 in
336 Fig. 4; Cornamusini et al., 2017; Veneri, 1986). In the footwall of the Valmarecchia ‘chaotic’
337 units, rock types exposed to the west of the UMSTZ (refer to Fig. 1) include the carbonate to
338 marly deposits accreted within the orogenic wedge. The outcropping stratigraphic succession
339 starts with the Calcare Massiccio Fm. (carbonate platform limestone, Upper Triassic - Lower
340 Jurassic) that represents the oldest formation exposed within the study area. This unit (unit 10 in
341 Fig. 4) is overlain by the Jurassic-Lower Cretaceous series that is mainly composed of cherty
342 limestone (Corniola Fm; unit 9 in Fig. 4) and pelagic micritic limestones (Maiolica Fm; unit 8 in
343 Fig. 4). Calcareous-marly sediments deposited during the Late Cretaceous to Oligocene consist
344 of marls (Marne a Fucoidi Fm; unit 7 in Fig. 4) and the Scaglia Group (unit 6 in Fig. 4). These
345 sediments are covered by Miocene, hemipelagic deposits of the Bisciaro Fm. (Aquitanian -
346 Burdigalian) and the Schlier Fm. (Langhian-Tortonian), both of which are mainly composed of
347 alternating marly limestones, marls and shales (unit 5 in Fig. 4). Unit 4 includes turbiditic
348 deposits that represent the fill of the Messinian foredeep, which developed to the east of the
349 UMSTZ in response to the eastward migration of the thrust front (Ricci Lucchi, 1986). The
350 deformed Messinian foredeep basin fill is presently preserved in the Marche foothills (Fig. 4). To
351 the east, Plio-Quaternary strata composed of clays and sands (unit 3) and conglomerates (unit 2)
352 cover the Messinian foredeep deposits, or locally rest unconformably directly on the calcareous-
353 marly succession (Bigi et al., 1997; Cantalamessa et al., 1986; Cantalamessa and di Celma, 2004;
354 Ori et al., 1991). The contact between the Plio-Quaternary foreland basin succession and the
355 older stratigraphic units is locally controlled by high angle faults (Deiana et al., 2002; Fig. 4).

356

357

358



359
 360 Fig. 4 - Geological sketch of UMAF (modified from Conti et al., 2020). The geologic units were grouped into 11 rock
 361 categories according to their lithology and stratigraphical position. Dotted black line limits the high K_{sn} value area of
 362 Fig. 11 (see Section 4.4).
 363

364

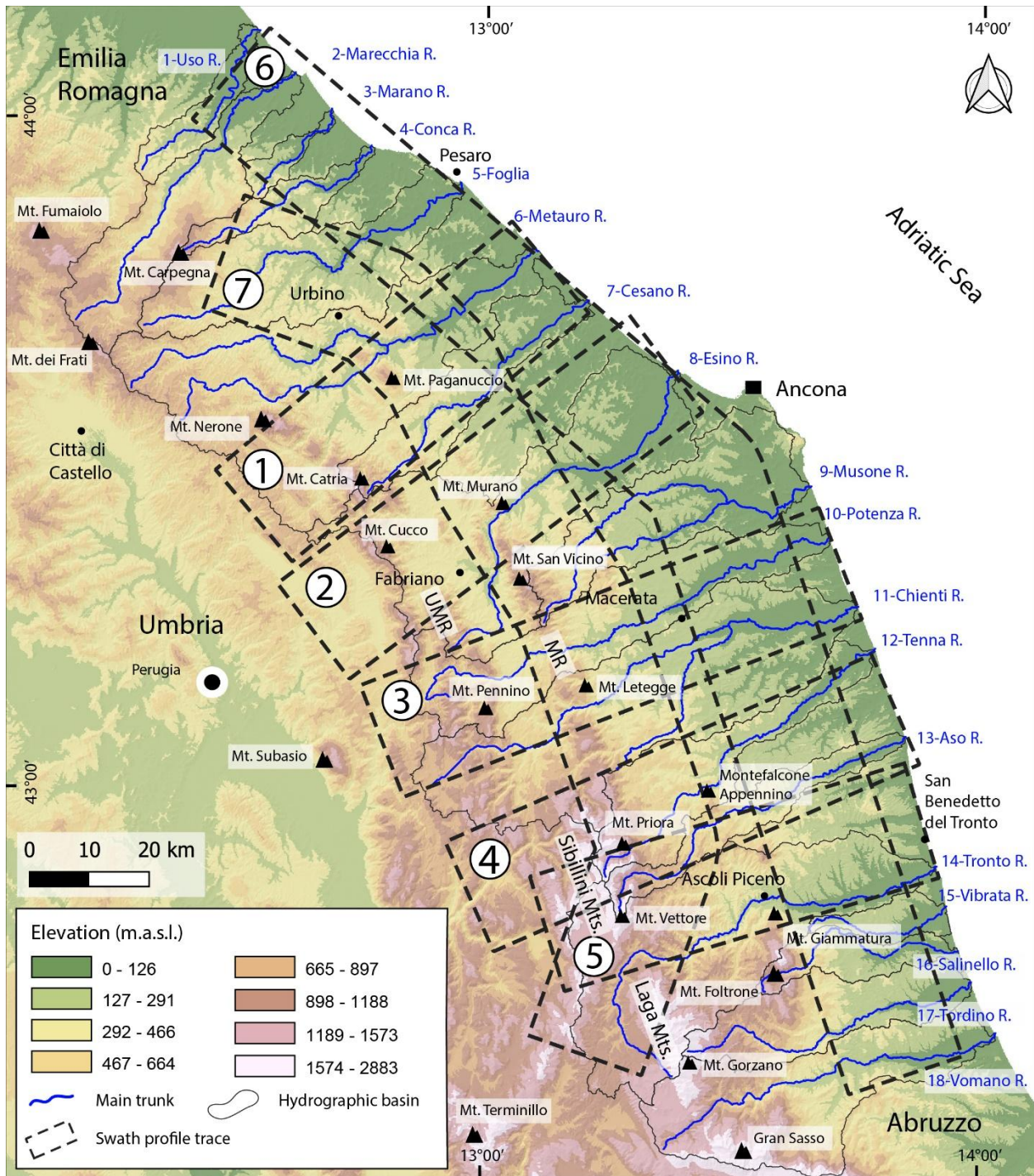
365 **4.3 Features of topography**

366 In the UMAF, the low elevation and low-gradient foothills (to the east of the UMSTZ) pass
367 to the mountainous landscape of the chain (to the west of the UMSTZ, Fig. 5). The location of
368 the UMSTZ is marked, in the swath profiles of Fig. 6, by the sudden drop in the maximum, mean
369 and the minimum elevation curves. This drop occurs at around 40 km in profiles 1, 2 and 3, and
370 at around 30 km and 20 km in profiles 4 and 5, respectively. The foothills exhibit a smooth
371 topography in the north (Fig. 5 and profiles 1 - 2 in Fig. 6) and a relatively rugged topography in
372 the south (Fig. 5 and profiles 3 to 5 in Fig. 6). Valleys to the south are narrower and Pleistocene
373 conglomerate deposits (unit 2 in Fig. 4), that are the stratigraphic cap of the foredeep section, are
374 preserved in some remnants of paleosurfaces. Parallel to the foothills, the chain exhibits lower
375 elevations and a smooth topography in the north. Here the highest peaks (e.g., Mt. Paganuccio,
376 976 m a.s.l.; Mt. Catria, 1702 m a.s.l.; Mt. Cucco, 1566 m a.s.l.; Mt. Murano, 882 m a.s.l.; Fig. 5
377 and profiles 1 - 2 in Fig. 6) correspond with the MR and the UMR formed by the Scaglia
378 carbonate units (unit 6 in Fig. 4). The ridges are aligned along two distinct NNW-SSE trends that
379 are separated by a large area where arenaceous and calcareous, marly, and clayey units crop out
380 (units 4 and 5, respectively, in Fig. 4). Towards the south, the chain is more elevated and rugged.
381 The MR and the UMR are separated by the Camerino Basin, where Messinian arenaceous
382 deposits crop out, in the area spanning from the Esino R. to the Chienti R. valleys (Fig. 5 and
383 profiles 2 - 3 in Fig. 6). The ridge to the NE (the MR) is carved in the Scaglia units (unit 6 in Fig.
384 4) and reaches a maximum elevation of 1021 m a.s.l. at Mt. Letegge (Fig. 5 and profile 3 in Fig.
385 6). To the SW, the UMR is carved both in the Scaglia and the Calcare Massiccio units (units 6
386 and 10, respectively, in Fig. 4) and its highest peak is Mt. Pennino (1571 m a.s.l.: Fig. 5 and
387 profile 3 in Fig. 6). Towards the south (from the Chienti R. to the Aso R. valleys) the MR and the
388 UMR converge, and the chain exhibits its highest elevation with the peaks of Mt. Priora (2333 m
389 a.s.l.) and Mt. Vettore (2467 m a.s.l.; Fig. 5 and profiles 4 -5 in Fig. 6), which are carved in the
390 Scaglia and the Calcare Massiccio units (units 6 and 10 , respectively, in Fig. 4). To the west of
391 Mt. Vettore peak (profile 5 in Fig. 6), high values in the maximum, mean and minimum
392 elevation curves are coupled with low values in the relief curve. This feature is associated with
393 the Castelluccio Quaternary basin in the hanging wall of the Mt. Vettore normal fault (Pierantoni
394 et al., 2013). The southernmost portion of the investigated area (e.g., from the Tronto R. to the

395 Vomano R. valleys), where Messinian arenaceous deposits crop out (unit 4 in Fig. 4), exhibits
396 high to very high elevations that culminate in the peak of Mt. Gorzano (2458 m.a.s.l.; Fig. 5).

397 Comparison of the profiles of Fig. 6 points to an overall increase of the elevation values
398 towards the south (i.e., from swath 1 to swath 5). Such a trend is also evident by swaths 6 and 7
399 (Fig. 6), which run parallel to the foothills and to the outer sector of the orogenic belt,
400 respectively. The highest peaks in the maximum elevation curves correspond with carbonate
401 units, and this trend is mirrored by the mean elevation curves. The minimum elevation curve is
402 smooth in the north (swaths 1, 2 and 3) with values not exceeding 500 m a.s.l., whereas in the
403 south (swaths 4 and 5) it exhibits two relevant peaks exceeding 1000 m a.s.l. These peaks
404 correspond with Mt. Priora (swath 4) and with the area to the west of Mt. Vettore (swath 5).
405 The relief curve mirrors the elevation curves, with the relief peaks that correspond with the
406 highest elevation peaks, and with increasing local relief towards the south (i.e., from profile 1 to
407 profile 5). Furthermore, swath profile 7 enhances the occurrence of three asymmetric, down to
408 the north, broad paleovalleys that are now dissected by the more narrowly spaced transverse
409 river valleys. The paleovalley to the north is centered around the Foglia River basin, the central
410 one spans from the Metauro River basin to Mt. San Vicino, and the southernmost one extends
411 from the Potenza River basin to Mt. Vettore.

412



413

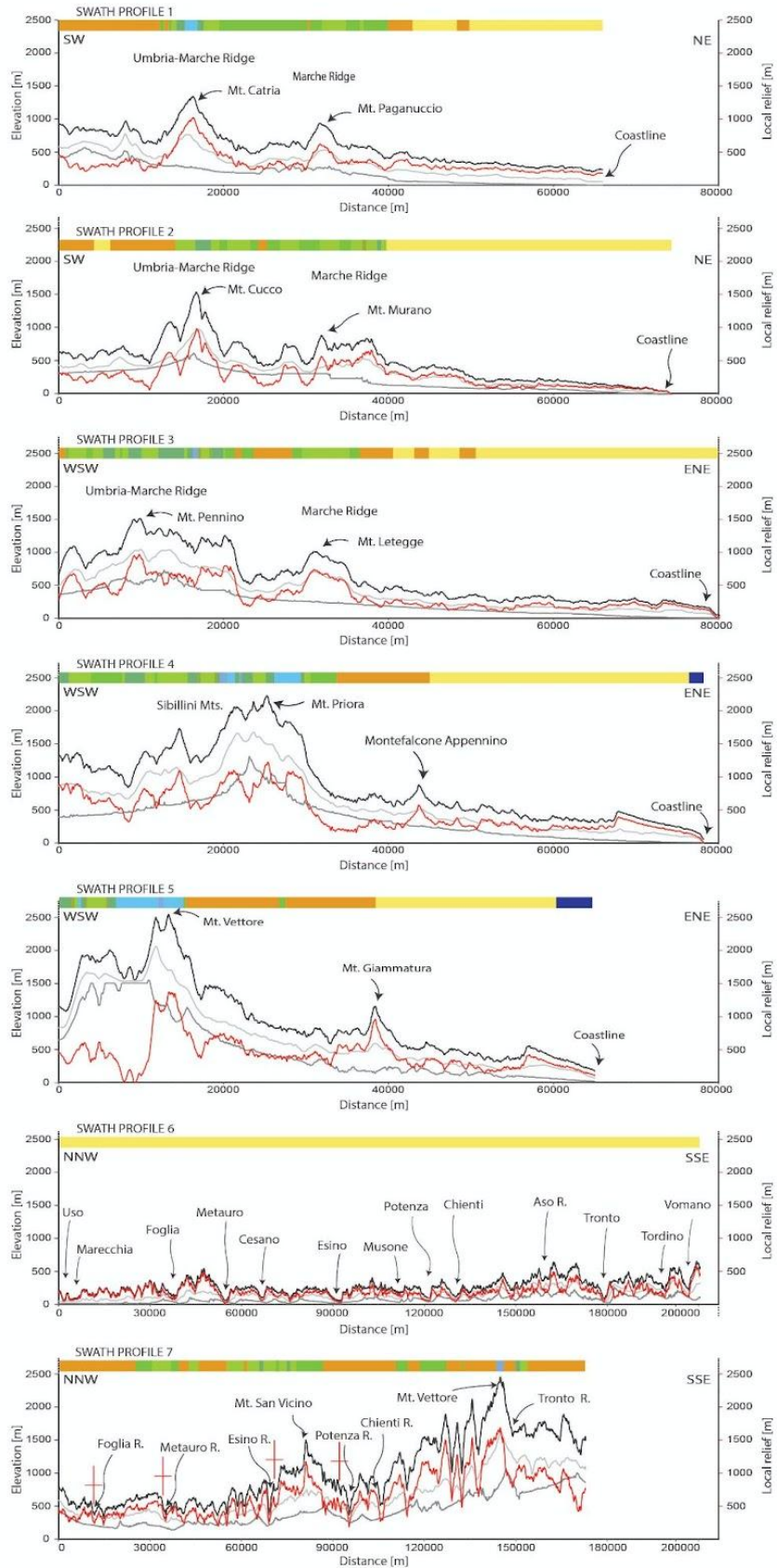
414

Fig. 5. Elevation map of the UMAF with location of the investigated main trunks, and correlative hydrographic basin. Black dotted boxes are the traces of swath profile in Fig. 6.

415

416

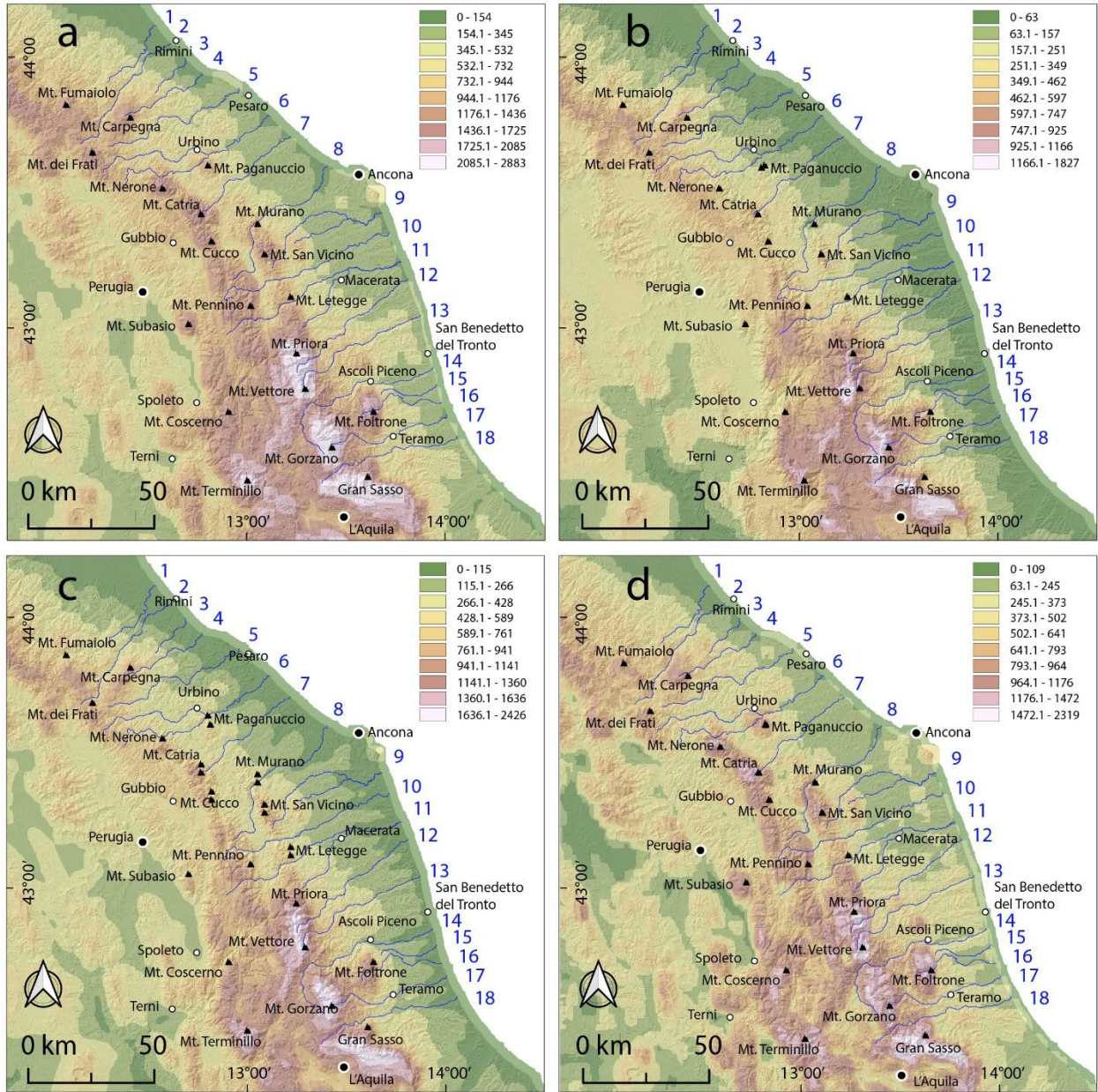
417



419
420 Fig. 6. Swath profiles within the Umbria-Marche Apennines and foothills (see Fig. 5 for the location). Swath
421 profiles 1 to 5 are SW-NE trending and run perpendicular to the chain. Swath profiles 6 and 7 are parallel to the
422 mountain front and perpendicular to river valleys. Black line indicates maximum elevation curve, gray line indicates
423 mean elevation curve, light gray line indicates minimum elevation curve, and red line indicates relief curve. The
424 colored bars above long river profiles represent the lithology of the bedrock reported in Fig. 4. Red crosses in swath
425 profile 7 indicate location of the transverse faults mapped in Fig. 1.

426
427 The above-described topography setting is also highlighted by the maximum (Fig. 7a),
428 minimum (Fig. 7b), and mean (Fig. 7c) elevation maps, as well as the local relief map (Fig. 7d).
429 All these maps point to the presence of a locus of high elevations and high relief to the south of
430 the investigated area (e.g., in the area between Mt. Vettore and Mt. Gorzano). This high
431 elevation area spans from the west of the UMSTZ to the east of it and includes different rock-
432 types, such as the carbonates of the Calcare Massiccio (unit 10 in Fig. 4) and the Messinian
433 arenaceous deposits (unit 4 in Fig. 4).

434



435
 436 Fig. 7. Elevation maps of the study area. (a) Maximum elevation map. (b) Minimum elevation map. (c) Mean
 437 elevation map. (d) Local relief map.
 438

439 **4.4 River long profiles and chi-plot analysis**

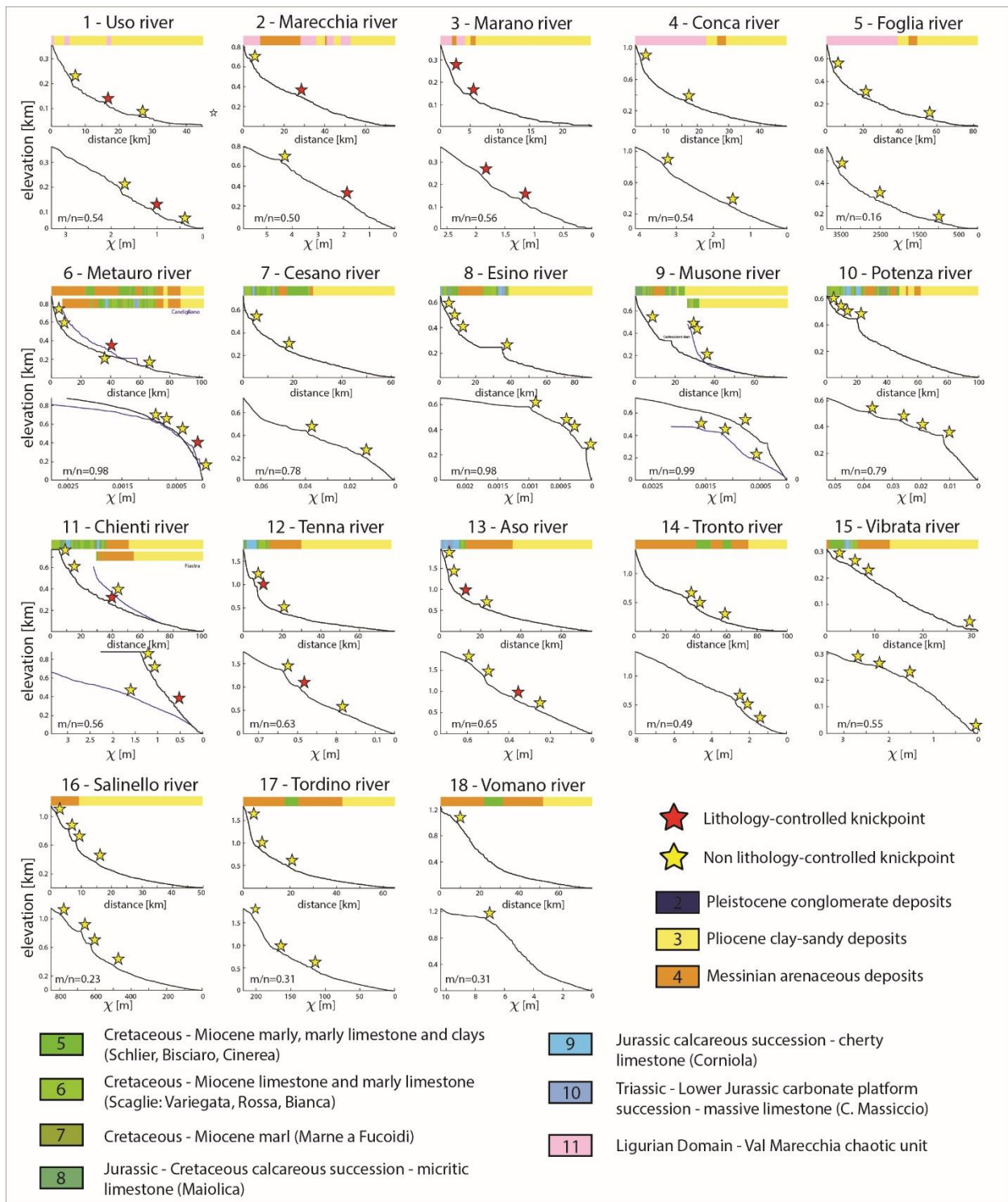
440 Fig. 8 shows river long profiles and chi-plots of the eighteen investigated rivers. To
 441 construct the chi-plots, we adopted the best fit m/n ratio at the basin scale (Section 3.2). River
 442 long profiles and chi-plots exhibit variable features along the strike of the UMAF. In the northern
 443 sector, e.g., in the area between the Uso River and the Foglia River (rivers 1 to 5 in Fig. 8), chi-

444 plots are rectilinear to slightly convex upward with the only exception of the Foglia River that
445 exhibits a concave upward chi plot. Several knickpoints are identified. Using as a reference the
446 lithological map of Fig. 4, some of the knickpoints have been classified as lithology-controlled
447 knickpoints because of their proximity to contacts. These knickpoints occur along the Uso River,
448 the Marecchia River and the Marano River (river 1, 2 and 3 in Fig. 8, respectively). On the
449 opposite, knickpoints along the Conca River and the Foglia River (rivers 4 and 5 in Fig. 8) are
450 not associated with lithological contacts (Figs. 8 and 9).

451 In the central sector of the investigated area, between the Metauro River and the Potenza
452 River (rivers 6 to 10; Fig. 8), the chi plots are characterized by convex shapes with knickpoints
453 that appear not associated with lithological contacts. However, a control by lithology may be
454 hypothesized for the knickpoint that occurs along the Candigliano River (a right tributary of the
455 Metauro River, 6; Fig. 8) to the west of Mt. Nerone (Fig. 9). Here the Calcare Massiccio (unit
456 10) outcrops in a deep gorge and passes laterally to marls, marly limestone and clay deposits of
457 the Bisciaro, Schlier and Cinerea Fms. (unit 5).

458 Rivers in the southern sector of the study area (rivers 11 to 18 in Fig. 8) show chi-plots with
459 shapes that vary from rectilinear and steep (11 - Fiastra River, a tributary of the Chienti River),
460 to convex or slightly convex (15 - Vibrata River; 11 - Chienti River; 14 - Tronto River) and to
461 rectilinear in the lower reach to convex upward in the upper reach (rivers 12, 13, 16, 17 and 18 in
462 Fig. 8). Most of the widespread knickpoints identified along these rivers have been classified as
463 non-lithology controlled knickpoints. Among the non-lithology controlled knickpoints, some in
464 the upper reaches of the Chienti, Salinello, Tordino and Vomano Rivers (rivers 11, 16, 17 and 18
465 in Fig. 8), occur at short distances from normal faults. Knickpoints classified as lithology
466 controlled are located along the Chienti (river 11, east of Mt. Letegge) and Aso (river 12,
467 northeast of Mt. Vettore) rivers at contacts between units 6 and 4, and along the Tenna River
468 (river 13, east of Mt. Priora) at the contact between units 5 and 6.

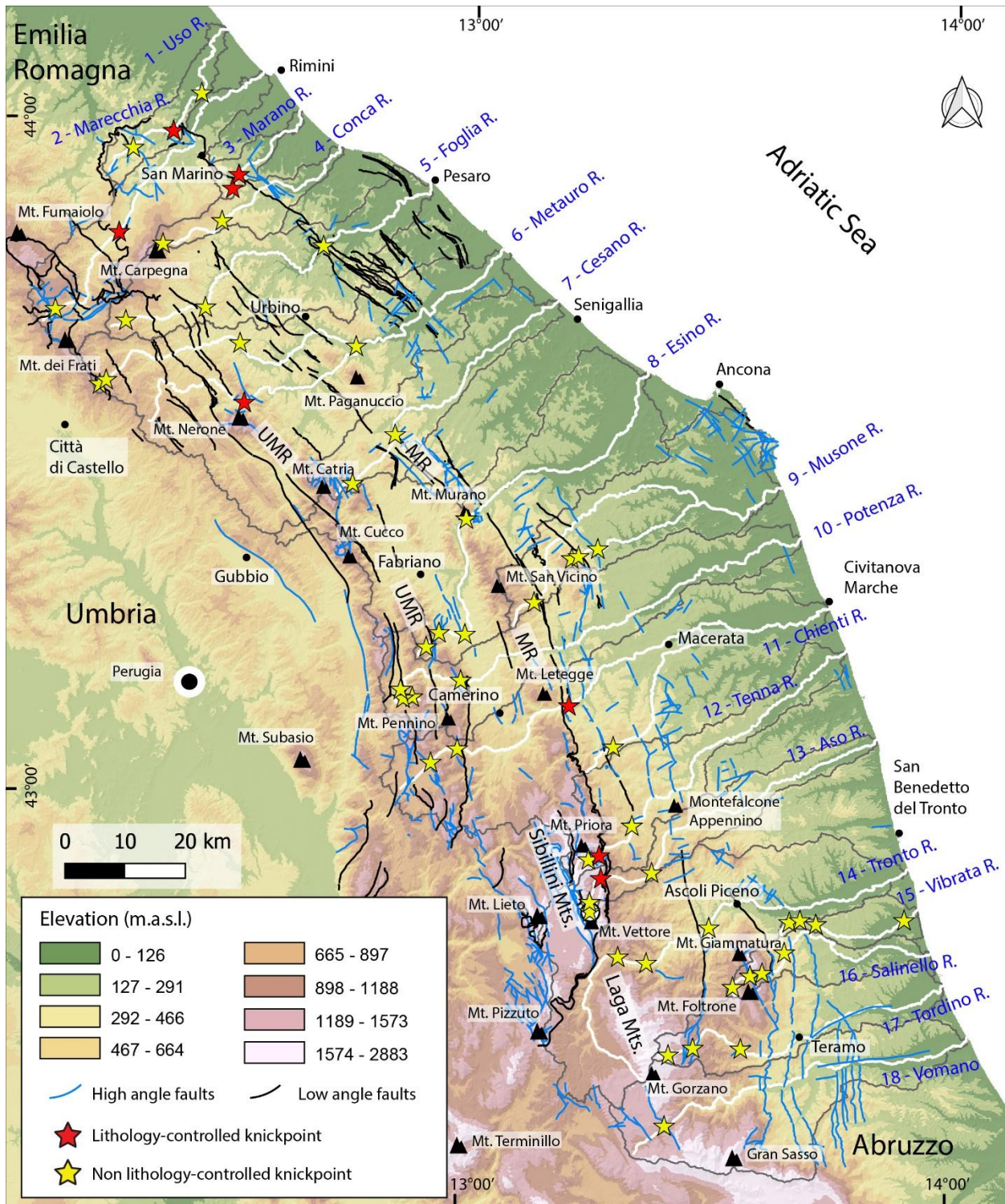
469



470
471
472
473
474

Fig. 8. Longitudinal profiles and chi plot of the 18 rivers analyzed in the present work. Chi-plots have been constructed using the best fit m/n ratio at the basin scale. The colored bars above long river profiles represent the lithology of the bedrock reported in Fig. 4.

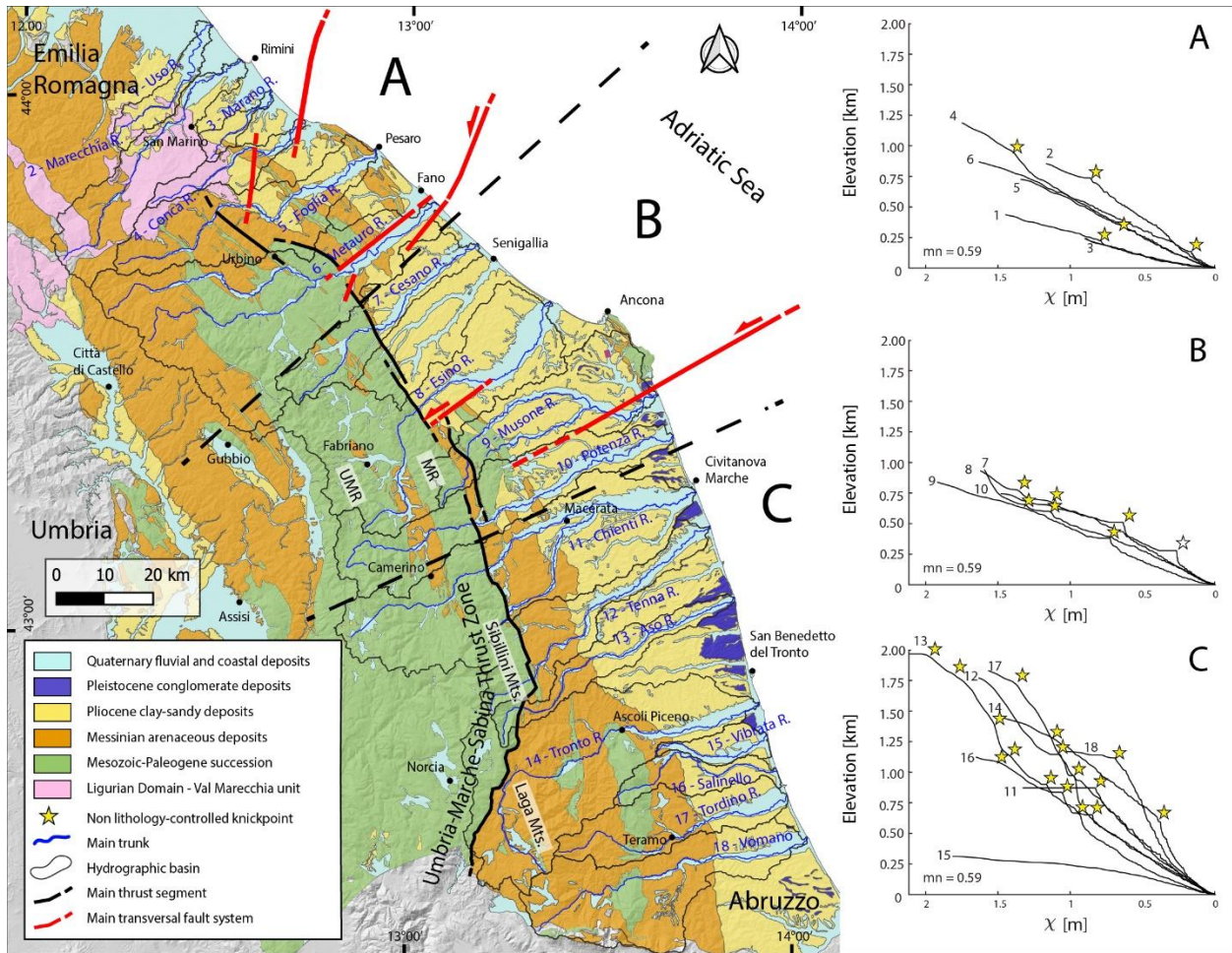
475 Fig. 9 shows the spatial distribution of knickpoints. Most of the non-lithology controlled
476 knickpoints are clustered in the southern sector of the UMAF (e.g., in the area spanning from the
477 Tenna River to the Vomano River), and are mainly located to the east of the UMSTZ, where the
478 Messinian arenaceous rocks (unit 4) crop out. Non-lithology controlled knickpoints located in
479 the chain units to the south of the UMAF occur only along the Tenna River and the Aso River
480 (number 12 and 13, respectively, in Figs. 8 and 9). On the opposite, to the north of the Chienti
481 River valley, non-lithology controlled knickpoints are clustered to the west of the UMSTZ. Such
482 knickpoints occur within the carbonate units, whereas knickpoints to the east of the UMSTZ
483 affect just the Uso, Foglia and Musone rivers (number 1, 5 and 9, respectively, in Figs. 8 and 9).
484
485



487 Fig. 9. Topographic map showing the knickpoints/knickzones spatial distribution along the 18 river channels
488 analyzed in the study area. The identified knickpoints are distinguished in lithology-controlled knickpoints and non-
489 lithology-controlled ones, using as a reference the geological map of Fig. 4. In this regard, red stars represent sharp
490 change in channel slope due to lithological contrast while yellow ones are the knickpoints related to possible base
491 level perturbation.

492
493 Fig. 10 shows chi-plots obtained with the average m/n value of 0.59. Chi-plots of rivers in
494 the northern UMAF (sector A in Fig. 10) have mainly rectilinear shapes (rivers 1 to 6) with some
495 slight convex upward segment in the upper reaches of rivers 2 and 4. In the central UMAF
496 (sector B in Fig. 10, and rivers 7 to 10), chi-plots have rectilinear to slightly convex upward
497 shapes. Rivers to the south of the UMAF (sector C in Fig. 10, and rivers 11 to 18) are
498 characterized by overall steeper chi-plots, which show enhanced convex upward segments that
499 locally pass to steep rectilinear segments in the lower reaches (rivers 11, 12, 13, 14, 16 and 17).
500 By the diagrams it is evident that in sector C non-lithology controlled knickpoints occur at
501 elevations ≥ 750 m and, however, higher than knickpoints in sectors A and B.

502
503



504
 505 Fig. 10. Geological sketch of Umbria-Marche Apennines and foothills (modified from Conti et al., 2020) with the
 506 major transversal structures (modified from Costa et al. 2023 and Pierantoni et al., 2019). On the right, chi plots of
 507 the main rivers of hydrographic basins (locations and numbering in Fig. 5), constructed using a best fit m/n value of
 508 0.59. Non-lithology-controlled knickpoints are also reported.

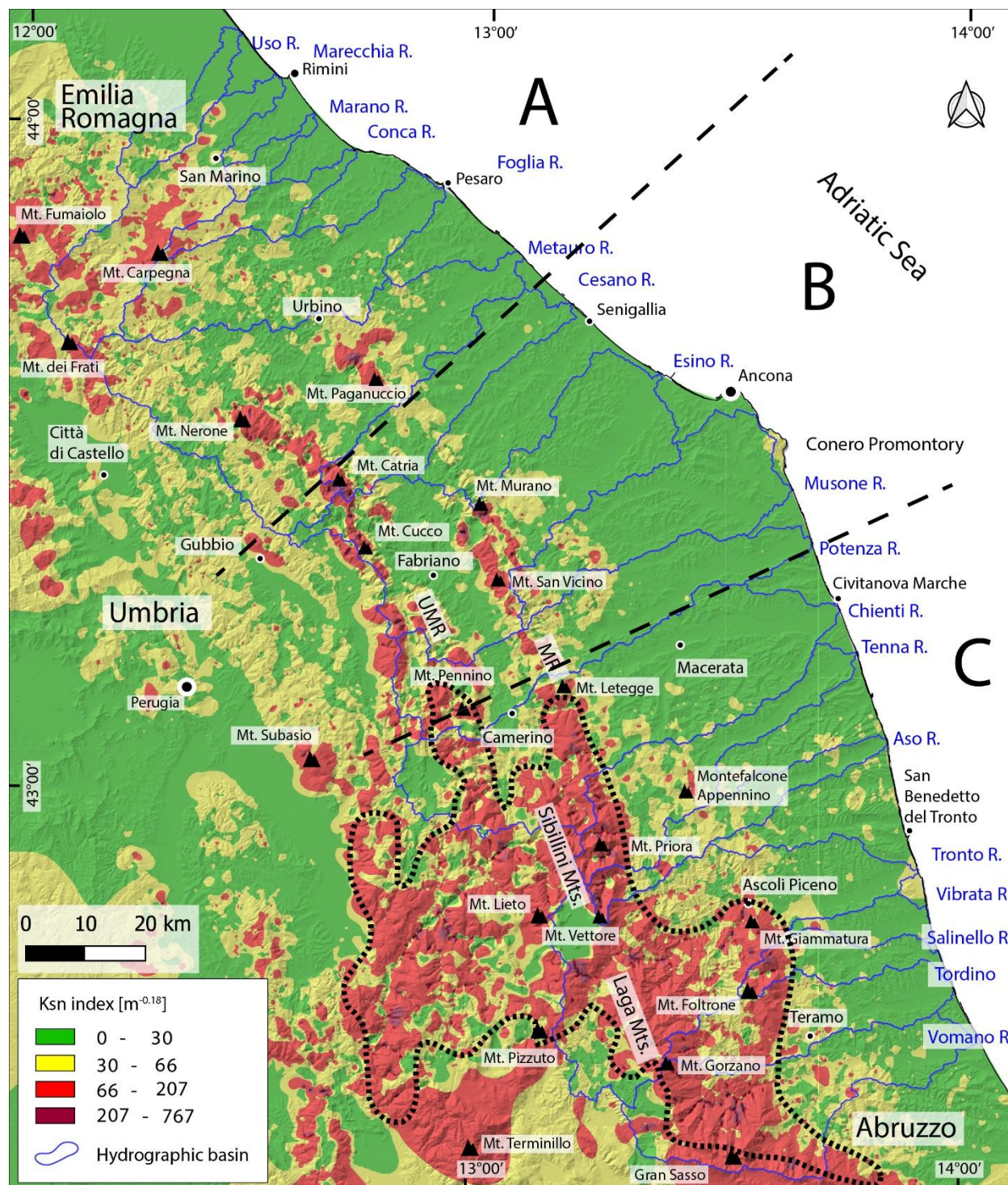
509
 510 We have also derived a χ map of the study area, which is shown in Supplementary Fig. 1. Details
 511 on the spatial distribution of this index are reported in the caption of this figure.

512
 513 **4.5 Ksn index**

514 Ksn values tend to increase towards the southwest, i.e., from the coastline to the foothills
 515 and to the mountain range (Fig. 11). Overall, the spatial distribution of the Ksn values follows
 516 the main features of the regional-scale topography. Low values are associated with the less
 517 elevated and low relief foothills, while the highest values are associated with areas characterized
 518 by high elevation and high local relief (Figs. 6 and 7). High Ksn values in the northern part of the

519 study region are associated with the MR and the UMR. Between the ridges, areas with low K_{sn}
 520 values occur locally in correspondence of some tectonic depressions where arenaceous and
 521 Quaternary continental deposits outcrop.

522
 523



524

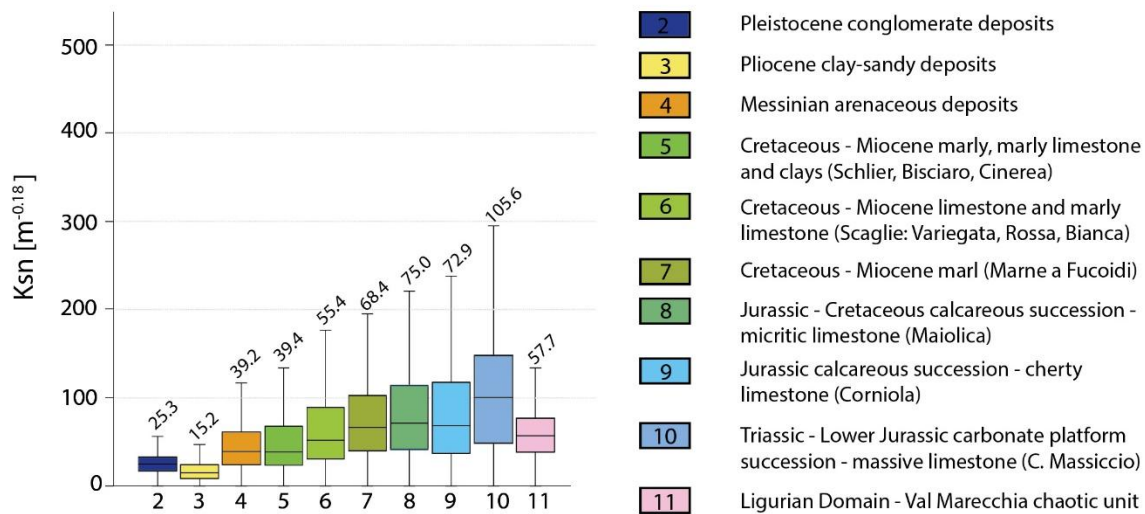
525 Fig. 11. Spatial distribution of K_{sn} index. Dashed black line limits the high K_{sn} value area. The sectors A, B and C of Fig. 10
 526 are also reported.

527

528 Considering the dependence of the K_{sn} on bedrock erodibility (Section 3.2), and to better
 529 investigate the relationship between the outcropping rocks and drainage properties inferred from
 530 the long-profile analyses (Section 4.2), we constructed box plots of the K_{sn} values as a function
 531 of lithology, using as a reference the rock groups distinguished in Fig. 4 (Fig. 12).

532

533



534

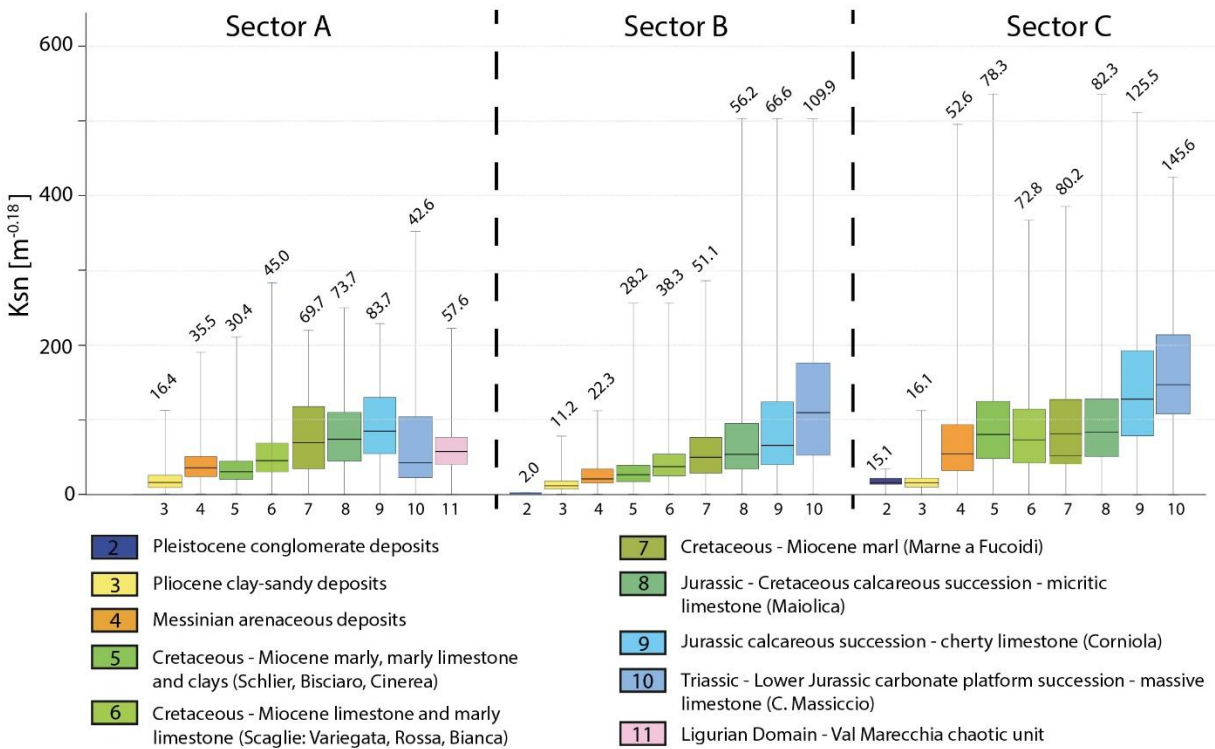
535 Fig. 12. Box plots showing distribution of the K_{sn} value as a function of lithology. The mean of the distribution is shown by the
 536 horizontal line within the box and it is repeated as the number above the top whisker. The top and bottom of the box are the 75th
 537 and 25th percentiles and the whiskers are the 95th and 5th percentiles.

538

539 By the compared box plots it appears that K_{sn} values respond to the lithological variability
 540 (Fig. 12). Although a net signature of each rock type is not identified, an association of the K_{sn}
 541 values with the lithological groups is evident. Overall, very low values are associated with the
 542 clastic deposits that outcrop in the foothills (units 2 and 3), with the lowest median value being
 543 associated with the clays and sands. Higher values characterize the mountain range units. For
 544 instance, in the entire study region, the highest K_{sn} values are associated with the carbonate
 545 rocks of the Maiolica and Corniola Fms. (units 8 and 9) and particularly, with the massive
 546 limestones of the Calcare Massiccio Fm. (unit 10). The marly and clayey rock-types (namely,
 547 units 5, 6 and 7) that are part of the Mesozoic-Cenozoic succession are coupled with lower K_{sn}

548 values. The Messinian arenaceous deposits (unit 4) exhibit low K_{sn} values that are comparable
 549 with those of the marls, marly limestone, and clays of the Schlier, Bisciario and Cinerea. Fms.
 550 (unit 5).

551 The map of Fig. 11 also shows that the K_{sn} values are affected by an along-strike variability
 552 and, particularly, increase from sector A to sector C. To analyze the pattern of the along-strike
 553 K_{sn} variability, we applied the box plot analysis as a function of lithology to each of the three
 554 sectors identified by the chi plot analysis (Fig. 13). The comparison of box plots constructed for
 555 sectors A, B and C indicates that, substantially, the statistical distribution of K_{sn} as a function of
 556 the lithological groups outcropping in the entire study area (and, particularly, the trend of the
 557 median values) is maintained in each of the sectors. In addition, the comparison between sectors
 558 A, B and C indicates that, for each rock type, the median value increases from sector A to sector
 559 C.
 560



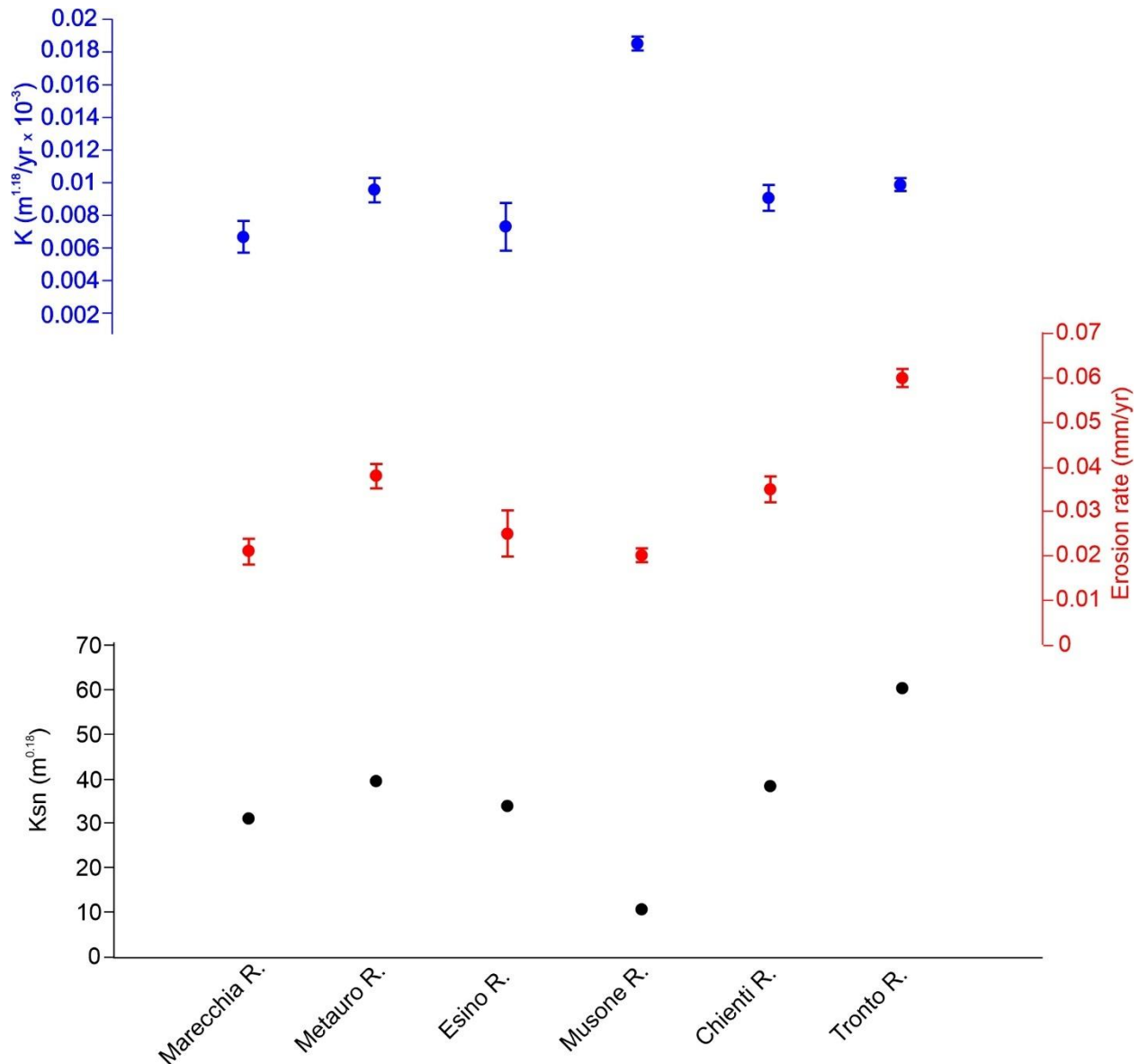
561
 562 Fig. 13. Box plots showing K_{sn} value as a function of lithology. Numbers on top of each box plot indicate the median value.
 563

564 **4.6 Spatial variation of the erodibility parameter (K)**

565 Values of the erodibility parameter (K) are reported in Tab. 1 and Fig. 14. This index has
 566 been calculated only for the drainage basins for which erosion rate estimation are reported in
 567 literature. The analysis points to a similar average K_{sn} value from the Marecchia River to the
 568 Chienti River (i.e., K_{sn} between 30 and 40), with the only exception of the Musone River that
 569 exhibits the lowermost value (K_{sn} value of 10.8). The Tronto River is characterized by the
 570 highest average K_{sn} value, this being almost double the value of rivers to the north of it. Erosion
 571 rate values range between 0.2 mm/yr (Musone R.) and 0.38 mm/yr, with the highest values in the
 572 Tronto River basin (0.6 m/yr⁻³). The erodibility (K) parameter exhibits similar values among all
 573 the analyzed drainage basins except for the Musone River, where it doubles the other values.
 574

Drainage basin	Average K _{sn} (m ^{0.18})	Erosion rate (mm/yr)	Error	K (m ^{1.18} /yr x 10 ⁻³)	Error	Source
Marecchia River	31.25	0.21	± 0.03	0.00672	± 0.00096	Guerra and Lazzari (2020)
Metauro River	39.65	0.38	± 0.03	0.009584	± 0.000757	Nesci et al. (2012)
Esino River	34.13	0.25	± 0.05	0.007325	± 0.001465	Nesci et al. (2012)
Musone River	10.8	0.2	± 0.002	0.018519	± 0.000185	Wegmann and Pazzaglia (2009)
Chienti River	38.44	0.35	± 0.03	0.009105	± 0.00078	Wegmann and Pazzaglia (2009); Coltorti et al. (1991)
Tronto River	60.69	0.6	± 0.02	0.009886	± 0.00033	Sembroni et al. (2020)

575 Tab. 1. Values of the erodibility parameter (K) for some of the investigated drainage basins,
 576
 577



578
 579 Fig. 14. Distribution of the Ksn, erosion rate and erodibility (K) among the selected drainage basins. Drainage basins
 580 are listed from north to south.

581
 582 **5 Discussion**

583 In our study, we performed an analysis of topography and river network of the Adriatic
 584 slope of the Umbria-Marche Apennines using multiple metrics and indices. We calculated the
 585 spatial distribution of elevation and parameters of the drainage network, i.e., river steepness and
 586 χ index, and compared these metrics with the outcropping rock types. Such an approach
 587 provided us with a key to unravel the tectonic vs. lithological signals and to identify areas with
 588 different behaviors in terms of vertical motions.

589

590 **5.1 Lithological control on topography and drainage network features**

591 The spatial coincidence of high vs. low values of parameters such as elevation and local
592 relief with outcrops of carbonate rocks (e.g., along the MR and the UMR) and clayey and/or
593 arenaceous rocks (e.g., the Camerino basin; Figs. 6 and 7), respectively, is a feature that the
594 UMAF share with other sectors of the Apennines. Like the central and southern Apennines
595 (Ascione and Cinque, 1999; Ascione et al., 2008; Buscher et al., 2017; Lanari et al., 2023;
596 Pazzaglia and Fisher, 2022), it appears that bedrock lithology exerts a strong control on the
597 features of topography of the UMAF mountain range.

598 The same is also inferred from the analysis of river long-profiles, which are well known to
599 respond to the control exerted by lithology (e.g., Duvall et al., 2004; Pazzaglia et al., 1998; Stock
600 and Montgomery, 1999). The extent to which the nature of the bedrock affects the features of
601 the drainage is inferred from the statistical analysis of the K_{sn} values (Fig. 12). This analysis,
602 consistently with findings from various morphoclimatic and morphotectonic settings (Bernard et
603 al., 2019; Clementucci et al., 2022; Seagren and Schoenbohm, 2019), indicates that such a
604 parameter is influenced by the resistance to erosion of the bedrock. In our instance, the K_{sn} box-
605 plot analysis allows a net distinction between the carbonate rocks of the Maiolica, Corniola and
606 Calcare Massiccio Fms. (units 8, 9 and 10; Fig. 12), which are all characterized by high K_{sn}
607 values, and rocks composed of arenaceous and marly-clayey lithologies (unit 4; Fig. 12).
608 Therefore, it is evident that the carbonate rocks of the Mesozoic-Paleogene Umbria-Marche
609 succession (namely, the Maiolica, Corniola and Calcare Massiccio Fms.) respond to erosion as
610 hard rocks relative to the softer marly-clayey portion of the same succession (namely, the
611 Schlier, Scaglia, and Bisciario Fms.) and the Messinian sandstones. The only exception is the
612 very low K_{sn} values associated with the Calcare Massiccio (unit 10) in sector A. These low
613 values are due to the limited areal distribution of the Calcare Massiccio that outcrops at low
614 elevation just in some gorges carved by the Metauro river (river 6). This implies that the low K_{sn}
615 values associated with the Calcare Massiccio in sector A are mainly affected by elevation and
616 local relief rather than lithology.

617 The coupled variations of the K_{sn}, elevation and relief parameters with lithology are indicative
618 of the main role exerted by differential erosion in the formation of the landscape of the uplifting
619 UMAF, as it has been inferred for the northern Apennines (Erlanger et al., 2021) and Crete (Ott

620 et al., 2019). However, the variability of bedrock lithology in the UMAF is much greater across
621 than along the strike of the investigated region (Fig. 4). This suggests that the along-strike
622 variation in topography and river network features may be considered as less affected by
623 outcropping rock types.

624 Consistently, the erodibility parameter (K) exhibits similar values from north to south
625 despite the southward increase in the erosion rate and in the average K_{sn} at the basin scale (Tab.
626 1 and Fig. 14). Therefore, the jump in K_{sn} values towards the south appears not merely
627 correlated with variable bedrock types. The only exception is the Musone River basin that
628 exhibits low K_{sn} value, erosion rate like the other investigated basins and the highest erodibility
629 (Fig. 14). This feature relates to the occurrence of a bedrock mainly composed of foredeep units
630 (Fig. 4) in contrast with the other investigated basins, which are mainly carved in the chain units.
631

632 **5.2 Along strike variation of uplift**

633 Elevation and its derivative parameters described in Section 4.3 all increase towards the
634 south, with maximum values occurring in the Sibillini Mts. and the Laga Mts (Figs. 5, 6 and 7).
635 This area corresponds with the high K_{sn} area shown in Fig. 11. The locus of high elevation, high
636 relief and high K_{sn} values to the south of the UMAF includes both carbonate rocks (units 8, 9
637 and 10 in Fig. 4), which culminate with the peak of Mt. Vettore, and arenaceous rocks that peak
638 with Mt. Gorzano (unit 4 in Fig. 4). The southward increase in K_{sn} values is clearly imaged by
639 the box plots in Fig. 13, which show a jump of this metric for all rock types in the southern
640 portion of the UMAF. Noteworthy, K_{sn} values associated with the Messinian arenaceous units
641 (unit 4) in sector C, besides being much higher than the correlative values in sectors A and B,
642 approach the K_{sn} values of calcareous and marly units (units 5, 6, 7 and 8).

643 This, in turn, supports the idea that lithology is not the first controlling factor in the
644 southward increasing elevation and in the steepness of the rivers (and chi plot patterns),
645 consistent with analyses by Lanari et al. (2023) that demonstrated that lithology alone cannot
646 explain the remarkable differences reported along the Apennines (e.g., elevation, river steepness,
647 etc.). Therefore, by our datasets it can be inferred that the southern portion of the study area
648 experienced larger uplift. This agrees with the findings of Racano et al. (2024) that recognized a
649 southward increasing trend in rock uplift in the central Apennines, with a maximum in the area
650 around the Sibillini Mts.

651 Focusing on the tectonic evolution of the UMAF (Section 2), the larger uplift recorded in the
652 southern part of the study area bears components related to both syn-orogenic shortening and
653 post-orogenic extension (e.g., the high elevation of Mt. Vettore peak). These two components are
654 not easily isolated, although the distribution of horizontal displacement associated with the
655 UMSTZ, which shows a marked maximum in the southern Marche region (~ 10 km in the Mt.
656 Vettore area) and values not exceeding 5 km in the northern Marche region (Mazzoli et al.,
657 2005), suggests that thrusting played a major role in producing structural elevation. Therefore,
658 the larger uplift experienced by the southern UMAF is partly inherited from pre-Quaternary
659 times, as it is also observed in the central Apennines more to the south (Ascione et al., 2008).
660 However, parameters of the drainage net, which is particularly sensitive to recent/active tectonic
661 perturbations (Kirby and Whipple, 2001; Racano et al., 2021; Whittaker et al., 2008), all support
662 the idea that the southward increase in surface uplift has continued during the Quaternary times.
663 Collectively, parameters such as non-lithology controlled knickpoints and Ksn index and their
664 spatial distribution, and chi-plots (Figs. 9, 10, 11 and 13), all indicate that rivers in the southern
665 portion of the UMAF are more perturbed relative to other rivers. Within such a regional-scale
666 trend, the stepped positions – independent from bedrock lithology - of the bottoms of the three
667 broad paleovalleys identified in swath profile 7 (Fig. 6; Section 4.3) suggest a discrete more than
668 gradual elevation increase towards the south. Discrete jumps in elevation occur at the boundaries
669 between sectors (A, B, C; Fig. 10) of the UMAF that feature different drainage net metrics.
670 Sector A is characterized by the lowest values of Ksn index (Fig. 13) and by rivers (rivers 1 to 6;
671 Figs. 8 and 10) that feature smooth long-profiles and rectilinear chi plots (Fig. 10), which suggest
672 that those rivers are substantially keeping pace with subdued uplift. In sector B the Ksn index is
673 characterized by mean values and river chi-plots (rivers 7 to 10; Figs. 8 and 10) that register only
674 some minor perturbation and are not far from keeping pace with moderate uplift. Sector C
675 includes the high Ksn area (Figs. 11 and 13) and river chi-plots that are either overall convex
676 upward or with convex upper reaches that pass to steep rectilinear lower reaches (Fig. 10).
677 Considering the large sizes of the convex upward reaches, the variable nature (carbonate and
678 arenaceous) of the bedrock that is incised, and the abundance of non-lithology controlled
679 knickpoints, the nature of the transient signals in the rivers that dissect sector C is reasonably
680 correlated with tectonic signals. These are not merely correlated with extensional faulting, as the
681 across-strike size of the area subject to faster uplift encompasses the area affected by normal

682 faulting and extends eastwards to involve the deformed foredeep. The transformed profiles of
683 rivers in Sector C, relative to those located more to the north in the UMAF, are generally steeper
684 even in their straight lower reaches. Such a feature would suggest (e.g., Perron and Royden,
685 2013) a tendency of rivers 11 to 18 to the attainment of equilibrium with uplift faster than those
686 one affecting the area to the north of sector C., This is consistent with estimates for the Chienti
687 and Tronto rivers basins by Sembroni et al. (2020) and Pazzaglia and Fischer (2022).
688 Accordingly, transient signals in Fig. 10 are clustered at higher elevation (≥ 750 m) in sector C
689 compared to sectors A and B. Assuming that knickpoints record the same unsteady base level fall
690 history, the difference of elevation of transient signals in sectors A and B compared to sector C is
691 indicative of uplift of sector C greater than uplift of sectors A and B.

692 Overall, our results are consistent with findings of recent works (e.g., Faccenna et al., 2014;
693 Fellin et al., 2022; Lanari et al. ,2023; Serpelloni et al., 2013; Racano et al., 2024) pointing to a
694 southward increase of uplift. These papers interpret the uneven uplift in terms of deep
695 geodynamic processes, without discussing the role of crustal transverse structures. Dynamic
696 support may not have a unique topographic fingerprint and if anything, the more parsimonious
697 explanation is that crustal structure changes significantly across NE-SW oriented zones, and it is
698 this crustal structure and crustal processes that are a better explanation for the observed
699 geomorphology. Our data provide new insights in the uplift pattern, being indicative of a
700 compartmentalization of the UMAF that is consistent with the occurrence of transversal
701 lineaments controlling differential uplift. Crucial to unravel such a behavior of the UMAF were
702 the (i) analysis of the along-strike features of elevation (i.e., swath n. 7 of Fig. 6), (ii) mutual
703 comparison among river network metrics, in particular chi-plot shapes and elevations of transient
704 signals (Fig. 10), (iii) box plots and whisker plots of Ksn values as a function of lithology (Fig.
705 13), and (iv) recognition of the net jumps of those metrics at the well-identified positions.

706

707 **5.3 The role of transversal structures**

708 Transversal structures are well known to occur in orogenic systems all over the world,
709 including the Apennines (Pascucci et al., 2007). The scale of these structures varies from the
710 common tear faults associated with individual thrust sheets and confined within thrust hanging-
711 wall blocks (Dahlstrom, 1970), to plate-scale transform faults. Within this wide range of scales,
712 fold and thrust belts may be compartmentalized by crustal or even lithospheric structures that are

713 not manifested by discrete fault zones at the surface but are unraveled by geophysical data and/or
714 geomorphological evidence. Tearing of the subducting slab and related focusing of the slab pull
715 force could result in transversal lithospheric structures impacting fold and thrust belt geology and
716 geomorphology (e.g., Handy et al., 2019, and references therein). This may be the case of the
717 northern-central Apennines, where a southward increasing uplift rate has been attributed to local
718 slab detachment beneath the central Apennines since late Pliocene/early Pleistocene times
719 (Faccenna et al., 2014; Fellin et al., 2022). Marked along-strike variations of relief evolution
720 could also result from delamination of the Adria lithosphere, a process recently inferred by
721 Menichelli et al. (2023) based on seismic tomography. In this model, belt topography is
722 dynamically sustained by mantle substitution generated during the delamination process.
723 According to the latter authors, delamination proceeded with different retreat velocity along the
724 mountain belt. The resulting irregular geometry could have triggered belt segmentation,
725 producing different sectors bounded by transversal structures.

726 The geodynamic processes discussed above may well play a role in along-strike
727 segmentation of the northern-central Apennines. However, greater uplift in the southern sector of
728 the UMAF, evidenced by recent literature and the analysis completed here, appears to be
729 essentially controlled by inherited (Late Miocene to Pliocene) crustal scale shortening rather than
730 dynamic support. The basement-involved thrust architecture of the mountain belt (Fig. 2) is fully
731 consistent with such an interpretation. Within our study area, the boundaries among sectors (A,
732 B, C) characterized by different active tectonic behavior, roughly coincide with major transversal
733 faults segmenting the outer portion of the fold and thrust belt in the Marche foothills and
734 adjacent offshore area (Fig. 1). This correlation suggests that such transversal ‘lineaments’ mark
735 the loci of long-lived, deep-seated fault zones that exert a major control on the active tectonic
736 behavior of large crustal blocks. The recent reactivation of inherited, transversal crustal faults in
737 the foreland plate has been unraveled in the southern Apennines by Bitonte et al. (2021). The
738 latter authors also documented fault propagation into the foreland basin deposits as a result of
739 basement fault reactivation. A similar process is envisaged to have occurred also in the present
740 study area, where pre-existing, deep-seated transversal faults of the foreland plate appear to have
741 controlled fold and thrust belt propagation and related segmentation of the deformed Plio-
742 Pleistocene foredeep (Centamore and Nisio, 2003; Costa et al., 2021; Costa et al. 2023;
743 Pierantoni et al., 2019). Long-term activity of such transversal faults likely involved: (i) their

744 development during Triassic to Early Jurassic times as extensional/oblique-slip faults within the
745 framework of continental rifting (e.g., Tavarnelli et al., 2019); (ii) their reactivation as strike-
746 slip/oblique-slip faults compartmentalizing the fold and thrust belt during forelandward
747 migration of shortening (Calamita et al., 1994; Calamita and Pizzi, 1994); and (iii) their
748 reactivation as extensional/oblique-slip faults in the hinterland of the eastward migrating fold and
749 thrust belt. Stages (ii) and (iii) above are both Neogene-Quaternary in age, extension following
750 shortening in both space and time. The results of this study document the influence of the
751 transversal lineaments on the drainage network and topography of the study area.

752 The fact that the crustal sectors (A, B, C) characterized by different active tectonic
753 behavior extend SW-ward into the axial zone of the mountain chain (i.e., also in the hanging wall
754 of the major thrust – the UMSTZ – that defines the mountain front), further suggests that the
755 transversal ‘lineaments’ mapped in the frontal part of the fold and thrust belt mark major crustal
756 structures extending beneath the high mountain chain. As the latter area is presently dominated
757 by ongoing extension, it may be envisaged that the deep-seated transversal structures interact
758 with the active normal faults, thus segmenting the Quaternary extensional system in the axial
759 zone of the chain. This is consistent with seismicity distribution, and with the abrupt northward
760 truncation of the events associated with the 2016-2017 Amatrice-Visso-Norcia and the 1997
761 Colfiorito seismic sequences (Fig. 3) along the boundary between block C and block B in Fig.
762 10. Moreover, recent studies based on instrumental seismicity (Mazzoli et al., 2014, 2015),
763 seismic interpretation (Costa et al., 2021) and paleoseismological evidence (Materazzi et al.,
764 2022) highlight that major transversal structures can also host moderate to significant seismic
765 events (e.g., the Mw 6.17, 1741 Fabriano earthquake; the Mw 4.68, 1972 Ancona earthquake).
766 The transversal structures are a likely source of these large Marche earthquakes that have no
767 obvious correlation to emergent normal or thrust faults.

768

769 **6 Conclusions**

770 A morphotectonic analysis of the topography and drainage network features was applied
771 in this study to discern the lithological and tectonic signatures on landscape evolution in the
772 Umbria-Marche Apennines and Foothills (central Italy). Topography and river network features
773 exhibit along-strike variations that are consistent with a southward increase of surface uplift
774 rather than bedrock variability. Differential uplift associated with three major crustal blocks was

775 identified, with surface uplift reaching its maximum in the southernmost one (Sibillini Mts. –
776 Laga Mts. area). Crucial to the detection of the UMAF uplift pattern was the identification of
777 discrete variations in the metrics we analyzed.

778 In the Marche foothills and Adriatic offshore, the boundaries among crustal blocks
779 characterized by different active tectonic behavior roughly coincide with major transversal faults
780 recently mapped by seismic interpretation. Our study indicates that the crustal blocks displaying
781 differential surface uplift extend westward into the axial zone of the mountain chain, which is
782 characterized by active extension and associated intense seismicity. Seismicity distribution,
783 including the pattern of the 2016-2017 earthquake sequence, is consistent with a
784 compartmentalization of the active extensional fault system in the axial zone of the mountain
785 chain. Therefore, it may be envisaged that the boundaries among the three major blocks
786 identified by morphotectonic analysis consist of long-lived, deep basement structures extending
787 beneath the allochthonous tectonic units located in the hanging wall of the main thrust fault that
788 controls the mountain front in the region. Such transversal basement structures interact with
789 extensional seismogenic faults at hypocentral depths, thus playing a major role in the
790 seismotectonic behavior of the study area. The UMAF are clearly segmented and traversed by
791 crustal-scale faults. These faults may be seismogenic and responsible for large, deadly
792 earthquakes that have been historically difficult to attribute to known, emergent faults.

793 The fact that the more uplifted area extends well beyond the footwall blocks of active
794 normal faults is consistent with the relief pattern being the result of regional tectonic processes
795 occurring on a much larger scale with respect to footwall uplift. This large-scale pattern of relief
796 evolution has been interpreted in terms of deep geodynamic processes affecting the segmented
797 subducting slab (e.g., Faccenna et al., 2014; Menichelli et al., 2023). Indeed, most of the recent
798 literature is all about dynamic support of the Apennines, with too little attention afforded to
799 crustal-scale processes including active extension and shortening. Although the two types of
800 ‘deep’ vs. ‘shallow’ processes are not mutually exclusive, the crustal structures discussed in this
801 study suggest that the uplift pattern of the UMAF is mostly the result of lithosphere deformation
802 – and particularly along-strike variations of crustal shortening mostly inherited from Late
803 Miocene to Pliocene times – rather than dynamic support.

804 Our results, besides challenging the prevailing paradigm for recent Apennines uplift and
805 surface strain by providing new insights into crustal-scale, along-strike segmentation of the belt

806 (including the axial zone and the extensional system active there), may contribute to a better
807 understanding of the complex tectonic behavior of active mountain belts in the Mediterranean
808 region and elsewhere.

809

810 **Data availability statement**

811 Data about the instrumental seismicity since 1985 derive from the Italian Seismological
812 Instrumental and Parametric Data-Base (<http://terremoti.ingv.it/iside> ISIDe -INGV) and from the
813 re-localized earthquakes by INGV Ancona (Cattaneo et al., 2017). Data about historical
814 earthquakes with $M > 5.0$ derive by the Parametric Catalog of Italian Earthquakes – CPTI15-
815 DBMI15 (Rovida et al., 2022). The 30 m NASA ASTER GDEM V2
816 (<https://asterweb.jpl.nasa.gov/gdem.asp>, last access on 8 December 2023) has been used for
817 morphotectonic analysis. Maps have been created using Arcgis © (<https://www.esri.com/it->
818 [it/arcgis/products/arcgis-online/overview](https://www.esri.com/it-arcgis/products/arcgis-online/overview)), Matlab
819 (<https://it.mathworks.com/products/matlab.html>) and CorelDraw
820 (<https://www.coreldraw.com/it/product/coreldraw/?topNav=it>).

821

822 **Acknowledgment**

823 This paper is part of the Ph.D. thesis of Simone Teloni at the University of Camerino (Supervisor
824 Prof. Chiara Invernizzi). We are grateful to the Associate Editor (Prof. Gideon Rosenbaum) and
825 two reviewers (Prof. Frank Pazzaglia and Dr. Dario Gioia) for their useful comments that helped
826 us to improve the manuscript.

827 **References**

- 828 Ascione, A., Ciarcia, S., Di Donato, V., Mazzoli, S., & Vitale, S. (2012). The Pliocene-
829 Quaternary wedge-top basins of southern Italy: An expression of propagating lateral slab tear
830 beneath the Apennines. *Basin Research*, 24(4), 456-474. [https://doi.org/10.1111/j.1365-
831 2117.2011.00534.x](https://doi.org/10.1111/j.1365-2117.2011.00534.x)
- 832 Ascione, A., & Cinque, A. (1999). Tectonics and erosion in the long-term relief history of
833 Southern Apennines (Italy). *Zeitschrift fur Geomorphologie, Suppl.-Bd.* 117, 1–15.
- 834 Ascione, A., Cinque, A., Miccadei, E., Villani, F., & Berti, C. (2008). The Plio-Quaternary uplift
835 of the Apennines Chain: new data from the analysis of topography and river valleys in Central
836 Italy. *Geomorphology*, 102, 105-118, doi:10.1016/j.geomorph.2007.07.022
- 837 Barchi, M. R., Alvarez, W., & Shimabukuro, D. H. (2012). The Umbria-Marche Apennines as a
838 double orogen: observations and hypotheses. *Italian Journal of Geosciences*, 131(2), 258-271.
839 <https://doi.org/10.3301/IJG.2012.17>
- 840 Barchi, M., Minelli, G., & Pialli, G. (1998). The CROP 03 profile: a synthesis of results on deep
841 structures of the Northern Apennines. *Memorie della Società Geologica Italiana*, 52, 383-400
- 842 Barchi, M. R., & Mirabella, F. (2009). The 1997–98 Umbria–Marche earthquake sequence:
843 “Geological” vs. “seismological” faults. *Tectonophysics*, 476(1-2), 170-179.
844 <https://doi.org/10.1016/j.tecto.2008.09.013>
- 845 Basili, R., & Barba, S. (2007). Migration and shortening rates in the northern Apennines, Italy:
846 Implications for seismic hazard. *Terra Nova*, 19(6), 462–468. [https://doi.org/10.1111/j.1365-
847 3121.2007.00772.x](https://doi.org/10.1111/j.1365-3121.2007.00772.x)
- 848 Basilici, M., Ascione, A., Megna, A., Santini, S., Tavani, S., Valente, E., & Mazzoli, S. (2020).
849 Active deformation and relief evolution in the western Lurestan region of the Zagros
850 mountain belt: new insights from tectonic geomorphology analysis and finite element
851 modeling. *Tectonics*, 39(12), e2020TC006402. <https://doi.org/10.1029/2020TC006402>
- 852 Bernard, T., Sinclair, H.D., Gailleton, B., Mudd, S.M., & Ford, M. (2019). Lithological control
853 on the post-orogenic topography and erosion history of the Pyrenees. *Earth and Planetary
854 Science Letters*, 518, 53-66. <https://doi.org/10.1016/j.epsl.2019.04.034>
- 855 Bigi, S., Cantalamessa, G., Centamore, E., Didaskalou, P., Micarelli, A., Nisio, S., Pennesi, T., &
856 Potetti, M. (1997). The periadriatic basin (Marche-Abruzzi sector, central Italy) during the
857 Plio-Pleistocene. *Giornale di Geologia*, 59(1-2), 245-259.

858 Bishop, P. (2007). Long-term landscape evolution: linking tectonics and surface processes. *Earth*
859 *Surface Processes and Landform*, 32(3), 329-365. <https://doi.org/10.1002/esp.1493>

860 Bitonte, R., Livio, F. A., Mazzoli, S., Bellentani, G., Di Cesare, L., Dall'Igna, M., Castelluccio,
861 A., & Scaramuzzo, E. (2021). Frontal accretion vs. foreland plate deformation: Discriminating
862 the style of post-collisional shortening in the Apennines. *Journal of Structural Geology*, 145,
863 104290. <https://doi.org/10.1016/j.jsg.2021.104290>

864 Brogi, A., Capezzuoli, E., Martini, I., Picozzi, M., & Sandrelli, F. (2014). Late Quaternary
865 tectonics in the inner Northern Apennines (Siena Basin, southern Tuscany, Italy) and their
866 seismotectonic implication. *Journal of Geodynamics*, 76, 25-45.
867 <https://doi.org/10.1016/j.jog.2014.03.001>

868 Bull, W. B. (2008). *Tectonic geomorphology of mountains: a new approach to paleoseismology*.
869 John Wiley & Sons. <https://doi.org/10.1002/9780470692318>

870 Bull, W.B. & McFadden, L.D. (1977) *Tectonic Geomorphology North and South of the Garlock*
871 *Fault, California*. In: D.O., Doehring (Eds.), *Geomorphology in Arid Regions: A Proceedings*
872 *Volume of the 8th Annual Geomorphology Symposium* (p. 115-138). Binghamton, NY: State
873 University of New York. <https://doi.org/10.4324/9780429299230-5>

874 Burbank, D. W., & Anderson, R. S. (2011). *Tectonic Geomorphology*. Chichester, United
875 Kingdom: John Wiley & Sons. <https://doi.org/10.1002/9781444345063>

876 Buscher, J. T., Ascione, A., & Valente, E. (2017). Decoding the role of tectonics, incision and
877 lithology on drainage divide migration in the Mt. Alpi region, southern Apennines, Italy.
878 *Geomorphology*, 276, 37-50. <https://doi.org/10.1016/j.geomorph.2016.10.003>.

879 Butler, R. W. H., Mazzoli, S., Corrado, S., De Donatis, M., Di Bucci, D., Gambini, R., Naso, G.,
880 Nicolai, C., Scrocca, D., Shiner, P., & Zucconi, V. (2004). Applying thick-skinned tectonic
881 models to the Apennine thrust belt of Italy— Limitations and implications, in McClay, K. R
882 (Eds.): *Thrust tectonics and hydrocarbon systems: AAPG Memoir 82*, p. 647 – 667.
883 <https://doi.org/10.1306/M82813C34>

884 Calamita, F., Cello, G., Deiana, G., & Paltrinieri, W. (1994). Structural styles, chronology rates
885 of deformation, and time-space relationships in the Umbria-Marche thrust system (central
886 Apennines, Italy). *Tectonics*, 13(4), 873-881. <https://doi.org/10.1029/94TC00276>

887 Calamita, F., Deiana, G., Invernizzi, C., & Pizzi, A. (1991). Tettonica. In: Marche Assessorato
888 urbanistica e ambiente (Eds.), *L'ambiente fisico delle Marche: geologia, geomorfologia e*
889 *idrogeologia* (69-80). Firenze, Italy: Ed. Selca.

890 Calamita, F., & Pizzi, A. (1994). Recent and active extensional tectonics in the southern Umbro-
891 Marchean Apennines (central Italy). *Memorie della Società Geologica Italiana*, 48, 541-548.

892 Calderoni, G., Della Seta, M., Fredi, P., Lupia Palmieri, E., Nesci, O., Savelli, D., & Troiani, F.
893 (2010). Late Quaternary geomorphological evolution of the Adriatic coast reach
894 encompassing the Metauro, Cesano and Misa river mouths (Northern Marche, Italy). *Geo*
895 *Acta Special Publication*, 3, 109-124.

896 Cantalamessa, G., Centamore, E., Chiocchini, U., Colalongo, M. L., Micarelli, A., Nanni, T.,
897 Pasini, G., Potetti, M., & Ricci Lucchi, F. (1986). Il Plio-Pleistocene delle Marche. *Studi*
898 *geologici camerti*, 61-81.

899 Cantalamessa, G., & Di Celma, C. (2004). Sequence response to syndepositional regional uplift:
900 insights from high-resolution sequence stratigraphy of late Early Pleistocene strata,
901 Periadriatic Basin, central Italy. *Sedimentary Geology*, 164 (3-4), 283-309.
902 <https://doi.org/10.1016/j.sedgeo.2003.11.003>

903 Castelli, V., & Monachesi, G. (2001). Seismic history and historical earthquake scenario for the
904 town of Fabriano (Central Italy). *Italian Geotechnical Journal*, 35(2), 36-46.

905 Cattaneo, M., Frapiccini, M., Ladina, C., Marzorati, S., & Monachesi, G. (2017). A mixed
906 automatic-manual seismic catalog for central-eastern Italy: Analysis of homogeneity. *Annals*
907 *of Geophysics*, 60(6). <https://doi.org/10.4401/AG-7333>

908 Centamore, E., Fumanti, F., & Nisio, S. (2002). The central-northern Apennines geological
909 evolution from Triassic to Neogene time. *Bollettino della Società Geologica Italiana.*, Vol.
910 *Spec. 1*, 181-197.

911 Centamore, E., & Nisio, S. (2003). Effects of uplift and tilting in the Central-Northern Apennines
912 (Italy). *Quaternary international*, 101, 93-101. [https://doi.org/10.1016/S1040-6182\(02\)00092-](https://doi.org/10.1016/S1040-6182(02)00092-7)
913 *7*

914 Centamore, E., & Rossi, D. (2009). Neogene-Quaternary tectonics and sedimentation in the
915 Central Apennines. *Italian Journal of Geosciences*, 128(1), 73-88.
916 <https://doi.org/10.3301/ijg.2009.128.1.73>

917 Chiaraluce, L., Amato, A., Cocco, M., Chiarabba, C., Selvaggi, G., Di Bona, M., ... & Ripepe,
918 M. (2004). Complex normal faulting in the Apennines thrust-and-fold belt: The 1997 seismic
919 sequence in central Italy. *Bulletin of the Seismological Society of America*, 94(1), 99-116.
920 <https://doi.org/10.1785/0120020052>

921 Cinque, A., Patacca, E., Scandone, P., & Tozzi, M. (1993). Quaternary kinematic evolution of
922 the Southern Apennines. Relationships between surface geological features and deep
923 lithospheric structures. <https://doi.org/10.4401/ag-4283>

924 Cipollari, P., Cosentino, D., & Gliozzi, E. (1999). Extension and compression related basins in
925 central Italy during the Messinian Lago-Mare event. *Tectonophysics*, 315(1-4), 163-185.
926 [https://doi.org/10.1016/S0040-1951\(99\)00287-5](https://doi.org/10.1016/S0040-1951(99)00287-5)

927 Civico, R., Pucci, S., Villani, F., Pizzimenti, L., de Martini, P. M., Nappi, R., & EMERGEO
928 Working Group (2018). Surface ruptures following the 30 October 2016 Mw 6.5 Norcia
929 earthquake, central Italy. *Journal of Maps*, 14(2).
930 <https://doi.org/10.1080/17445647.2018.1441756>

931 Clementucci, R., Ballato, P., Siame, L.L., Faccenna, C., Yaaqoub, A., Essaifi, A., Leanni, L., &
932 Guillou, V. (2022). Lithological control on topographic relief evolution in a slow tectonic
933 setting (Anti-Atlas, Morocco). *Earth and Planetary Science Letters*, 596, 117788.
934 <https://doi.org/10.1016/j.epsl.2022.117788>

935 Conti, P., Cornamusini, G., & Carmignani, L. (2020). An outline of the geology of the Northern
936 Apennines (Italy), with geological map at 1: 250,000 scale. *Italian Journal of Geosciences*,
937 139(2), 149-194. <https://doi.org/10.3301/IJG.2019.25>

938 Cornamusini, G., Conti, P., Bonciani, F., Callegari, I., & Martelli, L. (2017). Geology of the
939 ‘Coltre della Val Marecchia’ (Romagna-Marche Northern Apennines, Italy). *Journal of Maps*,
940 13(2), 207-218. <https://doi.org/10.1080/17445647.2017.1290555>

941 Cosentino, D., Asti, R., Nocentini, M., Gliozzi, E., Kotsakis, T., Mattei, M., Esu, D., Spadi, M.,
942 Tallini, M., Cifelli, F., Pennacchioni, M., Cavuoto, G., & Di Fiore, V. (2017). New insights
943 into the onset and evolution of the central Apennine extensional intermontane basins based on
944 the tectonically active L’Aquila Basin (central Italy). *GSA Bulletin*, 129(9-10), 1314-1336.
945 <https://doi.org/10.1130/B31679.1>

946 Costa, M., Chicco, J., Invernizzi, C., Teloni, S., & Pierantoni, P. P. (2021). Plio–Quaternary
947 Structural Evolution of the Outer Sector of the Marche Apennines South of the Conero
948 Promontory, Italy. *Geosciences*, 11(5), 184. <https://doi.org/10.3390/geosciences11050184>

949 Costa, M., Invernizzi, C., Penza, G., Teloni, S., & Pierantoni, P. P. (2023). Seismotectonic role
950 of transversal structures in the Plio-Quaternary evolution of the external Marche Apennines
951 (Italy). *Journal of the Geological Society*, 180(6), jgs2023-002.
952 <https://doi.org/10.1144/jgs2023-002>

953 Coward, M. P., De Donatis, M., Mazzoli, S., Paltrinieri, W., & Wezel, F. C. (1999). Frontal part
954 of the northern Apennines fold and thrust belt in the Romagna-Marche area (Italy): Shallow
955 and deep structural styles. *Tectonics*, 18(3), 559-574. <https://doi.org/10.1029/1999TC900003>

956 D'Agostino, N., Jackson, J. A., Dramis, F., & Funicello, R. (2001). Interactions between mantle
957 upwelling, drainage evolution and active normal faulting: an example from the central
958 Apennines (Italy). *Geophysical Journal International*, 147(2), 475-497.
959 <https://doi.org/10.1046/j.1365-246X.2001.00539.x>

960 D'Alessandro, L., Miccadei, E., & Piacentini, T. (2003). Morphostructural elements of central–
961 eastern Abruzzi: contributions to the study of the role of tectonics on the morphogenesis of
962 the Apennine chain. *Quaternary International*, 101, 115-124. [https://doi.org/10.1016/S1040-6182\(02\)00094-0](https://doi.org/10.1016/S1040-6182(02)00094-0)

963

964 Dahlstrom, C. D. (1970). Structural geology in the eastern margin of the Canadian Rocky
965 Mountains. *Bulletin of Canadian Petroleum Geology*, 18(3), 332-406.
966 <https://doi.org/10.35767/gscpgbull.18.3.332>

967 Das, S., Kandekar, A.M., Sangode, S.J. (2022). Lithologic control on geomorphic evolution of
968 the Central Western Gaths: an example from the Aghnashini catchment, Karnataka, India.
969 *Journal of the Geological Society of India*, 98, 451-459. <https://doi.org/10.1007/s12594-022-2001-6>

970

971 Deiana, G., Cello, G., Chiocchini, M., Galdenzi, S., Mazzoli, S., Pistolesi, E., Potetti, M.,
972 Romano, A., Turco, E., & Principi, M. (2002). Tectonic evolution of the external zones of the
973 Umbria-Marche Apennines in the Monte San Vicino-Cingoli area. *Bollettino Della Società
974 Geologica Italiana*, 121(1), 229-238.

975 Deiana, G., Mazzoli, S., Paltrinieri, W., Pierantoni, P. P., & Romano, A. (2003). Struttura del
976 fronte montuoso umbro-marchigiano-sabino. *Studi geologici camerti*, Vol. Spec. 2003, 15-36.

977 Delchiaro, M., Iacobucci, G., Della Seta, M., Gribenski, N., Piacentini, D., Ruscitto, V., ... &
978 Troiani, F. (2024). A fluvial record of late Quaternary climate changes and tectonic uplift
979 along the Marche Piedmont Zone of the Apennines: New insights from the Tesino River
980 (Italy). *Geomorphology*, 445, 108971. <https://doi.org/10.1016/j.geomorph.2023.108971>

981 Della Seta, M., Del Monte, M., Fredi, P., Miccadei, E., Nesci, O., Pambianchi, G., Piacentini, T.,
982 & Troiani, F. (2008). Morphotectonic evolution of the Adriatic piedmont of the Apennines: an
983 advancement in the knowledge of the Marche-Abruzzo border area. *Geomorphology*, 102(1),
984 119-129. <https://doi.org/10.1016/j.geomorph.2007.06.018>

985 Dewey, J. F. (1988). Extensional collapse of orogens. *Tectonics*, 7(6), 1123-1139.
986 <https://doi.org/10.1029/TC007i006p01123>

987 Dewey, J. F., Helman, M. L., Knott, S. D., Turco, E., & Hutton, D. H. W. (1989). Kinematics of
988 the western Mediterranean. *Geological Society, London, Special Publications*, 45(1), 265-283.
989 <https://doi.org/10.1144/GSL.SP.1989.045.01.15>

990 Di Biase, R. A., Whipple, K. X., Heimsath, A. M., & Ouimet, W. B. (2010). Landscape form and
991 millennial erosion rates in the San Gabriel Mountains, CA. *Earth and Planetary Science*
992 *Letters*, 289(1-2), 134-144. <https://doi.org/10.1016/j.epsl.2009.10.036>

993 Doglioni, C. (1995). Geological remarks on the relationships between extension and convergent
994 geodynamic settings. *Tectonophysics*, 252(1-4), 253-267. [https://doi.org/10.1016/0040-](https://doi.org/10.1016/0040-1951(95)00087-9)
995 [1951\(95\)00087-9](https://doi.org/10.1016/0040-1951(95)00087-9)

996 Doglioni, C., Dagostino, N., & Mariotti, G. (1998). Normal faulting vs regional subsidence and
997 sedimentation rate. *Marine and Petroleum Geology*, 15(8), 737-750.
998 [https://doi.org/10.1016/S0264-8172\(98\)00052-X](https://doi.org/10.1016/S0264-8172(98)00052-X)

999 Duvall, A., Kirby, E., & Burbank, D. (2004). Tectonic and lithologic controls on bedrock
1000 channel profiles and processes in coastal California. *Journal of Geophysical Research: Earth*
1001 *Surface*, 109(F3). <https://doi.org/10.1029/2003jf000086>

1002 Eizenhöfer, P. R., McQuarrie, N., Shelef, E., & Ehlers, T. A. (2019). Landscape response to
1003 lateral advection in convergent orogens over geologic time scales. *Journal of Geophysical*
1004 *Research: Earth Surface*, 124, 2056–2078. <https://doi.org/10.1029/2019JF005100>

1005 EMERGEIO Working Group (2016). Coseismic effects of the 2016 Amatrice seismic sequence:
1006 First geological results, *Annals of Geophysics Italy*, 59(5). <https://doi.org/10.4401/ag-7195>.

1007 England, P., & Molnar, P. (1990). Surface uplift, uplift of rocks, and exhumation of rocks.
1008 *Geology*, 18(12), 1173-1177. [https://doi.org/10.1130/0091-](https://doi.org/10.1130/0091-7613(1990)018<1173:SUUORA>2.3.CO;2)
1009 [7613\(1990\)018<1173:SUUORA>2.3.CO;2](https://doi.org/10.1130/0091-7613(1990)018<1173:SUUORA>2.3.CO;2)

1010 Erlanger, E. D., Rugenstein, J. K. C., Bufe, A., Picotti, V., & Willett, S. D. (2021). Controls on
1011 physical and chemical denudation in a mixed carbonate-siliciclastic orogen. *Journal of*
1012 *Geophysical Research: Earth Surface*, 126(8), e2021JF006064.
1013 <https://doi.org/10.1029/2021JF006064>

1014 Faccenna, C., Becker, T. W., Miller, M. S., Serpelloni, E., & Willett, S. D. (2014). Isostasy,
1015 dynamic topography, and the elevation of the Apennines of Italy. *Earth and Planetary Science*
1016 *Letters*, 407, 163-174. <https://doi.org/10.1016/j.epsl.2014.09.027>

1017 Fadul, C. M., Oliveira, P., Val, P. (2022). Ongoing landscape transience in the eastern Amazon
1018 Craton consistent with lithologic control of base level. *Earth Surface Processes and*
1019 *Landforms*, 47, 3117-3132. DOI: 10.1002/esp.5447.

1020 Fellin, M. G., San Jose, M., Faccenna, C., Willett, S. D., Cosentino, D., Lanari, R., ... & Maden,
1021 C. (2022). Transition from slab roll-back to slab break-off in the central Apennines, Italy:
1022 Constraints from the stratigraphic and thermochronologic record. *GSA Bulletin*, 134(7-8),
1023 1916-1930. <https://doi.org/10.1130/B36123.1>

1024 Ferrarini, F., Arrowsmith, J. R., Brozzetti, F., de Nardis, R., Cirillo, D., Whipple, K. X., ... &
1025 Cheng, F. (2021). Late quaternary tectonics along the peri-adriatic sector of the Apenninic
1026 Chain (Central-Southern Italy): Inspecting active shortening through topographic relief and
1027 fluvial network analyses. *Lithosphere*, 2021(1). <https://doi.org/10.2113/2021/7866617>

1028 Forte, A. M., Cowgill, E., & Whipple, K. X. (2014). Transition from a singly vergent to doubly
1029 vergent wedge in a young orogen: The Greater Caucasus. *Tectonics*, 33(11), 2077-2101.
1030 <https://doi.org/10.1002/2014TC003651>

1031 Frepoli, A., & Amato, A. (1997). Contemporaneous extension and compression in the Northern
1032 Apennines from earthquake fault-plane solutions. *Geophysical Journal International*, 129(2),
1033 368-388. <https://doi.org/10.1111/j.1365-246X.1997.tb01589.x>

1034 Galadini, F., & Messina, P. (2001). Plio-Quaternary changes of the normal fault architecture in
1035 the central Apennines (Italy). *Geodinamica Acta*, 14(6), 321-344.
1036 <https://doi.org/10.1080/09853111.2001.10510727>

1037 Gallen, S. F., & Wegmann, K. W. (2017). River profile response to normal fault growth and
1038 linkage: An example from the Hellenic forearc of south-central Crete, Greece. *Earth Surface*
1039 *Dynamics*, 5(1), 161-186. <https://doi.org/10.5194/esurf-5-161-2017>

1040 Gentili, B., Pambianchi, G., Aringoli, D., Materazzi, M., & Giacometti, M. (2017). Pliocene-
1041 Pleistocene geomorphological evolution of the Adriatic side of central Italy. *Geologica*
1042 *Carpathica*, 68(1), 6. <https://doi.org/10.1515/geoca-2017-0001>

1043 ISIDE Working Group. (2007). Italian Seismological Instrumental and Parametric Database
1044 (ISIDE). Istituto Nazionale di Geofisica e Vulcanologia (INGV).
1045 <https://doi.org/10.13127/ISIDE>

1046 Jaiswara, N.K., Kotluri, S.K., Pandey, P., & Pandey, A.K. (2020). MATLAB functions for
1047 extracting hypsometry, stream-length gradient index, steepness index, chi gradient of channel
1048 and swath profiles from digital elevation model (DEM) and other spatial data for landscape
1049 characterization. *Applied Computing and Geosciences*, 7, 100033.
1050 <https://doi.org/10.1016/j.acags.2020.100033>

1051 Keller, J. V. A., Minelli, G., & Piali, G. (1994). Anatomy of late orogenic extension: the
1052 Northern Apennines case. *Tectonophysics*, 238(1-4), 275-294. [https://doi.org/10.1016/0040-](https://doi.org/10.1016/0040-1951(94)90060-4)
1053 [1951\(94\)90060-4](https://doi.org/10.1016/0040-1951(94)90060-4)

1054 Keller, A. E., & Pinter, N. (2002). *Active Tectonics and Earthquakes, Uplift, and Landscape*, 2nd
1055 Ed., London, United Kingdom: Prentice Hall

1056 Kirby, E., & Whipple, K. (2001). Quantifying differential rock-uplift rates via stream profile
1057 analysis. *Geology*, 29(5), 415-418. [https://doi.org/10.1130/0091-](https://doi.org/10.1130/0091-7613(2001)029<0415:QDRURV>2.0.CO;2)
1058 [7613\(2001\)029<0415:QDRURV>2.0.CO;2](https://doi.org/10.1130/0091-7613(2001)029<0415:QDRURV>2.0.CO;2)

1059 Lanari, R., Reitano, R., Giachetta, E., Pazzaglia, F.J., Clementucci, R., Faccenna, C., & Fellin,
1060 M.G. (2022). Is the Anti-Atlas of Morocco still uplifting? *Journal of African Earth Sciences*,
1061 188, 104481. <https://doi.org/10.1016/j.jafrearsci.2022.104481>

1062 Lanari, R., Reitano, R., Faccenna, C., Agostinetti, N. P., & Ballato, P. (2023). Surface and
1063 Crustal Response to Deep Subduction Dynamics: Insights From the Apennines, Italy.
1064 *Tectonics*, 42(3), e2022TC007461. <https://doi.org/10.1029/2022TC007461>

1065 Lucente, F. P., Chiarabba, C., Cimini, G. B., & Giardini, D. (1999). Tomographic constraints on
1066 the geodynamic evolution of the Italian region. *Journal of Geophysical Research: Solid Earth*,
1067 104(B9), 20307-20327. <https://doi.org/10.1029/1999JB900147>

1068 Mancini, M., Cavinato, G. P., Blum, M., Marriot, S., & Leclair, S. (2005). The Middle Valley of
1069 the Tiber River, central Italy: Plio-Pleistocene fluvial and coastal sedimentation, extensional
1070 tectonics and volcanism. *Fluvial Sedimentology VII. IAS Spec. Publ*, 35, 373-396.
1071 <https://doi.org/10.1002/9781444304350.ch20>

1072 Martini, I. P., & Sagri, M. (1993). Tectono-sedimentary characteristics of Late Miocene-
1073 Quaternary extensional basins of the Northern Apennines, Italy. *Earth-Science Reviews*,
1074 34(3), 197-233. [https://doi.org/10.1016/0012-8252\(93\)90034-5](https://doi.org/10.1016/0012-8252(93)90034-5)

1075 Materazzi, M., Bufalini, M., Dramis, F., Pambianchi, G., Gentili, B., & Di Leo, M. (2022).
1076 Active tectonics and paleoseismicity of a transverse lineament in the Fabriano valley, Umbria-
1077 Marche Apennine (central Italy). *International Journal of Earth Sciences*, 111, 1539-1549.
1078 <https://doi.org/10.1007/s00531-022-02198-x>

1079 Mayer, L., Menichetti, M., Nesci, O., & Savelli, D. (2003). Morphotectonic approach to the
1080 drainage analysis in the North Marche region, central Italy. *Quaternary International*, 101,
1081 157-167. [https://doi.org/10.1016/S1040-6182\(02\)00098-8](https://doi.org/10.1016/S1040-6182(02)00098-8)

1082 Mazzoli, S., & Helman, M. (1994). Neogene patterns of relative plate motion for Africa-Europe:
1083 some implications for recent central Mediterranean tectonics. *Geol Rundsch*, 83, 464-
1084 468 <https://doi.org/10.1007/BF00210558>

1085 Mazzoli, S., Macchiavelli, C., & Ascione, A. (2014). The 2013 Marche offshore earthquakes:
1086 new insights into the active tectonic setting of the outer northern Apennines. *Journal of the*
1087 *Geological Society*, 171(4), 457-460. <https://doi.org/10.1144/jgs2013-091>

1088 Mazzoli, S., Santini, S., Macchiavelli, C., & Ascione, A. (2015). Active tectonics of the outer
1089 northern Apennines: Adriatic vs. Po Plain seismicity and stress fields. *Journal of*
1090 *Geodynamics*, 84, 62-76, <https://doi.org/10.1016/j.jog.2014.10.002>.

1091 Mazzoli, S., Pierantoni, P. P., Borraccini, F., Paltrinieri, W., & Deiana, G. (2005). Geometry,
1092 segmentation pattern and displacement variations along a major Apennine thrust zone, central
1093 Italy. *Journal of Structural Geology*, 27(11), 1940-1953.
1094 <https://doi.org/10.1016/j.jsg.2005.06.002>

1095 Mele, G., Rovelli, A., Seber, D., Hearn, T. M., & Barazangi, M. (1998). Compressional velocity
1096 structure and anisotropy in the uppermost mantle beneath Italy and surrounding regions.
1097 *Journal of Geophysical Research: Solid Earth*, 103(B6), 12529-12543.
1098 <https://doi.org/10.1029/98JB00596>

1099 Miccadei, E., Piacentini, T., & Buccolini, M. (2017). Long-term geomorphological evolution in
1100 the Abruzzo area, Central Italy: Twenty years of research. *Geologica Carpathica*, 68(1), 19.
1101 DOI: 10.1515/geoca-2017-0002

1102 Monachesi, G., Castelli, V., & Vasapollo, N. (1991). Historical earthquakes in Central Italy: case
1103 histories in the Marche area. *Tectonophysics*, 193(1-3), 95-107. [https://doi.org/10.1016/0040-](https://doi.org/10.1016/0040-1951(91)90191-T)
1104 [1951\(91\)90191-T](https://doi.org/10.1016/0040-1951(91)90191-T)

1105 Montuori, C., Cimini, G. B., & Favali, P. (2007). Teleseismic tomography of the southern
1106 Tyrrhenian subduction zone: New results from seafloor and land recordings. *Journal of*
1107 *Geophysical Research: Solid Earth*, 112(B3). <https://doi.org/10.1029/2005JB004114>

1108 Nesci, O., & Savelli, D. (2003). Diverging drainage in the Marche Apennines (central Italy).
1109 *Quaternary International*, 101, 203-209. [https://doi.org/10.1016/S1040-6182\(02\)00102-7](https://doi.org/10.1016/S1040-6182(02)00102-7)

1110 Nesci, O., Savelli, D., & Troiani, F. (2012). Types and development of stream terraces in the
1111 Marche Apennines (central Italy): a review and remarks on recent appraisals.
1112 *Géomorphologie: relief, processus, environnement*, 18(2), 215-238.
1113 <https://doi.org/10.4000/geomorphologie.9838>

1114 Obaid, A. K., & Allen, M. B. (2019). Landscape expressions of tectonics in the Zagros fold-and-
1115 thrust belt. *Tectonophysics*, 766, 20–30. <https://doi.org/10.1016/j.tecto.2019.05.024>

1116 Ori, G. G., Serafini, G., Visentin, C., Ricci Lucchi, F., Casnedi, R., Colalongo, M. L., & Mosna,
1117 S. (1991). The Pliocene-Pleistocene Adriatic Foredeep (Marche and Abruzzo, Italy): an
1118 integrated approach to surface and subsurface geology. In 3rd EAPG Conference, Adriatic
1119 foredeep field trip guide book (pp. 26-30). Florence, Italy: EAPG and AGIP.

1120 Ott, R. F., Gallen, S. F., Caves Rugenstein, J. K., Ivy-Ochs, S., Helman, D., Fassoulas, C., ... &
1121 Willett, S. D. (2019). Chemical versus mechanical denudation in meta-clastic and carbonate
1122 bedrock catchments on Crete, Greece, and mechanisms for steep and high carbonate
1123 topography. *Journal of Geophysical Research: Earth Surface*, 124(12), 2943-2961.
1124 <https://doi.org/10.1029/2019JF005142>

1125 Pace, P., Scisciani, V., Calamita, F., Butler, R. W., Iacopini, D., Eserime, P., & Hodgson, N.
1126 (2015). Inversion structures in a foreland domain: seismic examples from the Italian Adriatic
1127 Sea. *Interpretation*, 3(4), SAA161-SAA176. <https://doi.org/10.1190/INT-2015-0013.1>

1128 Pascucci, V.; Martini, I.P.; Sagri, M.; Sandrelli, F.; Nichols, G. (2007). Effects of transverse
1129 structural lineaments on the Neogene-Quaternary basins of Tuscany (inner Northern

1130 Apennines, Italy). *Sediment. Process. Environ. Basins*, 38, 155–182.
1131 <https://doi.org/10.1002/9781444304411.ch8>

1132 Patacca, E., Sartori, R., & Scandone, P. (1990). Tyrrhenian basin and Apenninic arcs: kinematic
1133 relations since late Tortonian times. *Memorie della Società Geologica Italiana*, 45, 425-451.

1134 Pazzaglia, F. J., & Fisher, J. A. (2022). A reconstruction of Apennine uplift history and the
1135 development of transverse drainages from longitudinal profile inversion. In *From the Guajira
1136 Desert to the Apennines, and from Mediterranean Microplates to the Mexican Killer Asteroid:
1137 Honoring the Career of Walter Alvarez*. Geological Society of America.
1138 [https://doi.org/10.1130/2022.2557\(09\)](https://doi.org/10.1130/2022.2557(09))

1139 Pazzaglia, F. J., Gardner, T. W., & Merritts, D. J. (1998). Bedrock fluvial incision and
1140 longitudinal profile development over geologic time scales determined by fluvial terraces.
1141 *Geophysical Monograph-American Geophysical Union*, 107, 207-236.
1142 <https://doi.org/10.1029/GM107p0207>

1143 Pérez-Peña, J. V., Al-Awabdeh, M., Azañón, J. M., Galve, J. P., Booth-Rea, G., & Notti, D.
1144 (2017). SwathProfiler and NProfiler: Two new ArcGIS Add-ins for the automatic extraction
1145 of swath and normalized river profiles. *Computers & Geosciences*, 104, 135-150.
1146 <https://doi.org/10.1016/j.cageo.2016.08.008>

1147 Perron, J. T., & Royden, L. (2013). An integral approach to bedrock river profile analysis. *Earth
1148 surface processes and landforms*, 38(6), 570-576. <https://doi.org/10.1002/esp.3302>

1149 Pezzo, G., Billi, A., Carminati, E., Conti, A., De Gori, P., Devoti, R., Lucente, F. P., Palano, M.,
1150 Petracchini, L., Serpelloni, E., Tavani, S., & Chiarabba, C. (2023). Seismic source
1151 identification of the 9 November 2022 Mw 5.5 offshore Adriatic sea (Italy) earthquake from
1152 GNSS data and aftershock relocation. *Scientific Reports*, 13, 11474.
1153 <https://doi.org/10.1038/s41598-023-38150-5>

1154 Piacentini, T., & Miccadei, E. (2014). The role of drainage systems and intermontane basins in
1155 the Quaternary landscape of the Central Apennines chain (Italy). *Rendiconti Lincei*, 25, 139-
1156 150. <https://doi.org/10.1007/s12210-014-0312-2>

1157 Pierantoni, P. P., Chicco, J., Costa, M., & Invernizzi, C. (2019). Plio-Quaternary transpressive
1158 tectonics: a key factor in the structural evolution of the outer Apennine–Adriatic system, Italy.
1159 *Journal of the Geological Society*, 176(6), 1273-1283. <https://doi.org/10.1144/jgs2018-199>

1160 Pierantoni, P.P., Deiana, G., & Galdenzi, S. (2013). Stratigraphic and structural features of the
1161 Sibillini mountains (Umbria-Marche Apennines, Italy). *Italian Journal of Geosciences*,
1162 132(3), 497-520. <https://doi.org/10.3301/IJG.2013.08>

1163 Piromallo, C., & Morelli, A. (2003). P wave tomography of the mantle under the Alpine-
1164 Mediterranean area. *Journal of Geophysical Research: Solid Earth*, 108(B2).
1165 <https://doi.org/10.1029/2002JB001757>

1166 Racano S., Fubelli, G., Ernesto, C., Bonasera, M., & Francesco, D. (2020). Geomorphological
1167 detection of surface effects induced by active blind thrusts in the southern Abruzzi peri-
1168 Adriatic belt (Central Italy). *Geografia Fisica e Dinamica Quaternaria*, 43, 3-13.
1169 [10.4461/GFDQ.2020.43.1](https://doi.org/10.4461/GFDQ.2020.43.1)

1170 Racano, S., Schildgen, T.F., Cosentino, D., Miller, S. R. (2021). Temporal and Spatial Variations
1171 in Rock Uplift From River-Profile Inversions at the Central Anatolian Plateau Southern
1172 Margin. *Journal of Geophysical Research: Earth Surface*, 126, e2020JF006027.
1173 <https://doi.org/10.1029/2020JF006027>

1174 Racano, S., Van der Beek, P. A., Schildgen, T. F., Faccenna, C., Buleo Tebar, V., Cosentino, D.
1175 (2024). Slab driven Quaternary rock-uplift and topographic evolution in the northern-central
1176 Apennines from linear inversion of the drainage system. *Geochemistry, Geophysics,*
1177 *Geosystems*, 25, e2024GC011592. <https://doi.org/10.1029/2024GC011592>

1178 Ricci Lucchi, F. (1986). The Oligocene to Recent foreland basins of the northern Apennines. In
1179 *Foreland basins* (Vol. 8, pp. 105-139). Blackwell Scientific Oxford.

1180 Rovida, A., Locati, M., Camassi, R., Lolli, B., Gasperini, P., & Antonucci, A. (2022). *Catalogo*
1181 *Parametrico dei Terremoti Italiani CPTI15, versione 4.0.*
1182 <https://doi.org/10.13127/cpti/cpti15.4>

1183 Royden, L., & Perron, T. J. (2013). Solutions of the stream power equation and application to the
1184 evolution of river longitudinal profiles. *Journal of Geophysical Research: Earth Surface*,
1185 118(2), 497-518. <https://doi.org/10.1002/jgrf.20031>

1186 San Jose, M., Rugenstein, J. K. C., Cosentino, D., Faccenna, C., Fellin, M. G., Ghinassi, M., &
1187 Martini, I. (2020). Stable isotope evidence for rapid uplift of the central Apennines since the
1188 late Pliocene. *Earth and Planetary Science Letters*, 544, 116376.
1189 <https://doi.org/10.1016/j.epsl.2020.116376>

1190 Santini, S., Basilici, M., Invernizzi, C., Jablonska, D., Mazzoli, S., Megna, A., Pierantoni, P.P.
1191 (2021). Controls of Radiogenic Heat and Moho Geometry on the Thermal Setting of the
1192 Marche Region (Central Italy): An Analytical 3D Geothermal Model. *Energies*, 14, 6511.
1193 <https://doi.org/10.3390/en14206511>

1194 Santini, S., Mazzoli, S., Megna, A., & Candela, S. (2016). Thermal Structure of the Outer
1195 Northern Apennines along the CROP-03 Profile. *Journal of Geography and Geology*, 8(4).
1196 [10.5539/jgg.v8n4p1](https://doi.org/10.5539/jgg.v8n4p1)

1197 Santini, S., Saggese, F., Megna, A., & Mazzoli, S. (2011). A note on central-northern Marche
1198 seismicity: new focal mechanisms for events recorded in years 2003-2009. *Bollettino di*
1199 *Geofisica Teorica ed Applicata*, 52(4). <https://doi.org/10.4430/bgta0025>

1200 Schildgen, T. F., Cosentino, D., Caruso, A., Buchwaldt, R., Yildirim, C., Bowring, S. A., Rojay,
1201 B., Echtler, H., Strecker, M. R. (2012). Surface expression of eastern Mediterranean slab
1202 dynamics: Neogene topographic and structural evolution of the southwest margin of the
1203 Central Anatolian Plateau, Turkey. *Tectonics*, 31(2). <https://doi.org/10.1029/2011TC003021>

1204 Schwanghart, W., & Kuhn, N. J. (2010). TopoToolbox: A set of Matlab functions for
1205 topographic analysis. *Environmental Modelling & Software*, 25(6), 770-781.
1206 <https://doi.org/10.1016/j.envsoft.2009.12.002>

1207 Schwanghart, W., & Scherler, D. (2014). TopoToolbox 2–MATLAB-based software for
1208 topographic analysis and modeling in Earth surface sciences. *Earth Surface Dynamics*, 2(1),
1209 1-7. <https://doi.org/10.5194/esurf-2-1-2014>

1210 Scisciani, V., Agostini, S., Calamita, F., Pace, P., Cilli, A., Giori, I., & Paltrinieri, W. (2014).
1211 Positive inversion tectonics in foreland fold-and-thrust belts: a reappraisal of the Umbria–
1212 Marche Northern Apennines (Central Italy) by integrating geological and geophysical data.
1213 *Tectonophysics*, 637, 218-237. <https://doi.org/10.1016/j.tecto.2014.10.010>

1214 Scotti, V. N., Molin, P., Faccenna, C., Soligo, M., & Casas-Sainz, A. (2014). The influence of
1215 surface and tectonic processes on landscape evolution of the Iberian Chain (Spain):
1216 Quantitative geomorphological analysis and geochronology. *Geomorphology*, 206, 37-57.
1217 <https://doi.org/10.1016/j.geomorph.2013.09.017>

1218 Seagren, E.G., & Schoenbohm, L.M. (2019). Base level and lithologic control of drainage
1219 reorganization in the Sierra de las Planchadas, NW Argentina. *Journal of Geophysical*
1220 *Research: EarthSurface*, 124, 1516–1539. <https://doi.org/10.1029/2018JF004885>

1221 Sembroni, A., Molin, P., Soligo, M., Tuccimei, P., Anzalone, E., Billi, A., Franchini, S., Ranaldi,
1222 M., & Tarchini, L. (2020). The uplift of the Adriatic flank of the Apennines since the Middle
1223 Pleistocene: New insights from the Tronto River basin and the Acquasanta Terme Travertine
1224 (central Italy). *Geomorphology*, 352, 106990.
1225 <https://doi.org/10.1016/j.geomorph.2019.106990>

1226 Serpelloni, E., Faccenna, C., Spada, G., Dong, D., & Williams, S. D. (2013). Vertical GPS
1227 ground motion rates in the Euro-Mediterranean region: New evidence of velocity gradients at
1228 different spatial scales along the Nubia-Eurasia plate boundary. *Journal of Geophysical*
1229 *Research: Solid Earth*, 118(11), 6003-6024. <https://doi.org/10.1002/2013JB010102>

1230 Spakman, W. (1990). Tomographic images of the upper mantle below central Europe and the
1231 Mediterranean. *Terra Nova*, 2(6), 542-553. <https://doi.org/10.1111/j.1365-3121.1990.tb00119.>

1232 Spakman, W., & Wortel, R. (2004). A tomographic view on western Mediterranean
1233 geodynamics. In *The TRANSMED Atlas. The Mediterranean region from crust to mantle:*
1234 *Geological and geophysical framework of the Mediterranean and the surrounding areas* (pp.
1235 31-52). Berlin, Heidelberg: Springer Berlin Heidelberg. [https://doi.org/10.1007/978-3-642-](https://doi.org/10.1007/978-3-642-18919-7_2)
1236 [18919-7_2](https://doi.org/10.1007/978-3-642-18919-7_2)

1237 Stock, J. D., & Montgomery, D. R. (1999). Geologic constraints on bedrock river incision using
1238 the stream power law. *Journal of Geophysical Research: Solid Earth*, 104(B3), 4983-4993.
1239 <https://doi.org/10.1029/98JB02139>

1240 Stucchi, M., Monachesi, G., & Mandrelli, F. M. (1991). Investigation of 18th century seismicity
1241 in central Italy in the light of the 1741 Fabriano earthquake. *Tectonophysics*, 193(1-3), 65-82.
1242 [https://doi.org/10.1016/0040-1951\(91\)90189-Y](https://doi.org/10.1016/0040-1951(91)90189-Y)

1243 Tavarnelli, E., Scisciani, V., Patruno, S., Calamita, F., Pace, P., & Iacopini, D. (2019). The role
1244 of structural inheritance in the evolution of fold-and-thrust belts: insights from the Umbria-
1245 Marche Apennines, Italy. In: Koeberl, C., Bice, D.M. (Eds.), *250 Million Years of Earth*
1246 *History in Central Italy: Celebrating 25 Years of the Geological Observatory of Coldigioco.*
1247 *Geological Society of America, Special Paper*, 542, 191-211,
1248 [https://doi.org/10.1130/2019.2542\(10\).](https://doi.org/10.1130/2019.2542(10))

1249 Turco, E., Macchiavelli, C., Penza, G., Schettino, A., & Pierantoni, P. P. (2021). Kinematics of
1250 deformable blocks: application to the opening of the tyrrhenian basin and the formation of the
1251 apennine Chain. *Geosciences*, 11(4), 177. <https://doi.org/10.3390/geosciences11040177>

1252 Valente, E., Buscher, J. T., Jourdan, F., Petrosino, P., Reddy, S. M., Tavani, S., Corradetti, A., &
1253 Tavani, S. (2019). Constraining mountain front tectonic activity in extensional setting from
1254 geomorphology and Quaternary stratigraphy: A case study from the Matese ridge, southern
1255 Apennines. *Quaternary Science Reviews*, 219, 47-67.
1256 <https://doi.org/10.1016/j.quascirev.2019.07.001>

1257 Vannoli, P., Basili, R., & Valensise, G. (2004). New geomorphic evidence for anticlinal growth
1258 driven by blind-thrust faulting along the northern Marche coastal belt (central Italy). *Journal*
1259 *of Seismology*, 8, 297-312. <https://doi.org/10.1023/B:JOSE.0000038456.00574.e3>

1260 Vannoli, P., Vannucci, G., Bernardi, F., Palombo, B., & Ferrari, G. (2015). The source of the 30
1261 October 1930 M w 5.8 Senigallia (Central Italy) earthquake: A convergent solution from
1262 instrumental, macroseismic, and geological data. *Bulletin of the Seismological Society of*
1263 *America*, 105(3), 1548-1561. <https://doi.org/10.1785/0120140263>

1264 Wegmann, K. W., & Pazzaglia, F. J. (2009). Late Quaternary fluvial terraces of the Romagna
1265 and Marche Apennines, Italy: Climatic, lithologic, and tectonic controls on terrace genesis in
1266 an active orogen. *Quaternary Science Reviews*, 28(1–2), 137–165.
1267 <https://doi.org/10.1016/j.quascirev.2008.10.006>

1268 Westaway, R. (1993). Quaternary uplift of southern Italy. *Journal of Geophysical Research:*
1269 *Solid Earth*, 98(B12), 21741-21772. <https://doi.org/10.1029/93JB01566>

1270 Whipple, K. X., Wobus, C., Crosby, B., Kirby, E., & Sheehan, D. (2007). New tools for
1271 quantitative geomorphology: Extraction and interpretation of stream profiles from digital
1272 topographic data. *GSA short course*, 506,
1273 Http://Geomorphtools.Org/Tools/StPro/Tutorials/StPro_UserGuidees_Final.Pdf

1274 Whittaker, A. C., Attal, M., Cowie, P. A., Tucker, G. E., & Roberts, G. (2008). Decoding
1275 temporal and spatial patterns of fault uplift using transient river long profiles.
1276 *Geomorphology*, 100(3-4), 506-526. <https://doi.org/10.1016/j.geomorph.2008.01.018>

1277 Wiemer, S. (2001). A software package to analyze seismicity: ZMAP. *Seismological Research*
1278 *Letters*, 72(3), 373-382. <https://doi.org/10.1785/gssrl.72.3.373>

1279 Wortel, M. J. R., & Spakman, W. (2000). Subduction and slab detachment in the Mediterranean-
1280 Carpathian region. *Science*, 290(5498), 1910-1917. DOI: 10.1126/science.290.5498.1910
1281